



Geochemistry and U–Pb detrital zircon dating of Paleozoic graywackes in East Junggar, NW China: Insights into subduction–accretion processes in the southern Central Asian Orogenic Belt

Xiaoping Long ^{a,b}, Chao Yuan ^{a,b,*}, Min Sun ^c, Inna Safonova ^d, Wenjiao Xiao ^{a,e}, Yujing Wang ^b

^a Xinjiang Research Center for Mineral Resources, Chinese Academy of Sciences, Urumqi 830011, China

^b State Key Laboratory of Isotope Geochemistry, Guangzhou Institute of Geochemistry, Chinese Academy of Sciences, Guangzhou 510640, China

^c Department of Earth Sciences, The University of Hong Kong, Pokfulam Road, Hong Kong, China

^d Institute of Geology and Mineralogy, SB RAS, Novosibirsk 630090, Russia

^e State Key Laboratory of Lithospheric Evolution, Institute of Geology and Geophysics, Chinese Academy of Sciences, Beijing 100029, China

ARTICLE INFO

Article history:

Received 29 November 2010

Received in revised form 15 May 2011

Accepted 22 May 2011

Available online 13 June 2011

Handling Editor: R.D. Nance

Keywords:

Detrital zircons

Provenance

Tectonics

Central Asian Orogenic Belt

Junggar

ABSTRACT

The southern Central Asian Orogenic Belt (CAOB) is characterized by multiple and linear accretionary orogenic collages, including Paleozoic arcs, ophiolites, and accretionary wedges. A complex history of subduction–accretion processes makes it difficult to distinguish the origin of these various terranes and reconstruct the tectonic evolution of the southern CAOB. In order to provide constraints on the accretionary history, we analyzed major and trace element compositions of Paleozoic graywackes from the Huangcaopo Group (HG) and Kubusu Group (KG) in East Junggar. The HG graywackes have relatively low Chemical Index of Alteration (CIA) values (50 to 66), suggesting a source that underwent relatively weak chemical weathering. The identical average Index of Compositional Variability (ICV) values (~1.1) for both the KG and HG samples point to an immature source for the Paleozoic graywackes in East Junggar, which is consistent with an andesitic–felsic igneous source characterized by low La/Th ratios and relatively high Hf contents. These graywackes are geochemically similar to continental island arc sediments and therefore were probably deposited at an active continental margin. U–Pb dating of detrital zircons from the lower subgroup of the HG yielded a young age peak at ~440 Ma, indicating a post–Early Silurian depositional age. However, the youngest populations of detrital zircons from the KG graywackes and the upper subgroup of the HG yielded ²⁰⁶Pb/²³⁸U ages of ~346 Ma and ~355 Ma, respectively, which suggest a post–Early Carboniferous depositional age. Because of similarities of rock assemblages, these two units should be incorporated into the Early Carboniferous Nanmingshui Formation. The detrital zircon age spectrum of the Early Paleozoic HG graywackes resembles that of the Habahe sediments in the Chinese Altai, which suggests that the ocean between East Junggar and the Chinese Altai was closed before the deposition of the sediments and that the Armantai ophiolite was emplaced prior to the Early Devonian. The differences in age spectra for detrital zircons from the post–Early Carboniferous graywackes in East Junggar and the Harlik arc indicate that the emplacement of the Kalamaili ophiolite postdates the Early Carboniferous. Therefore, a long–lasting northward subduction–accretion process is suggested for the formation of East Junggar and the reconstruction of the Early Paleozoic evolution of the southern CAOB.

© 2011 International Association for Gondwana Research. Published by Elsevier B.V. All rights reserved.

1. Introduction

The Central Asian Orogenic Belt (CAOB), also termed the Altaiids, is a large accretionary orogenic belt bounded by the Siberian Craton to the north and the Tarim–North China Craton to the south (Fig. 1, inset A; Şengör et al., 1993). This orogenic belt was formed by Early Neoproterozoic to Late Paleozoic subduction–accretion processes,

which resulted in accretion of island arcs, ophiolites, other supra-subduction units, and terranes with Precambrian crystalline basement to the southern margin of the Siberian Craton (Şengör and Natal'in, 1996; Buslov et al. 2001; Badarch et al. 2002; Khain et al. 2002, 2003; Xiao et al. 2003, 2009, 2010; Dobretsov et al., 2004; Safonova et al., 2004; Yakubchuk, 2004; Helo et al., 2006; Kröner et al., 2007; Windley et al., 2007). The geodynamic affinities of these various terranes are critical to rebuilding the evolution history of the CAOB. Clastic sediments hold key information about their source materials, tectonic settings and crustal growth events (e.g. Bhatia and Taylor, 1981; Bhatia and Crook, 1986; Roser and Korsch, 1986; McLennan et al., 1990). The geochemistry of sedimentary rocks and the geochronology of their detrital zircons were previously used to reconstruct the

* Corresponding author at: State Key Laboratory of Isotope Geochemistry, Guangzhou Institute of Geochemistry, Chinese Academy of Sciences, Guangzhou 510640, China. Tel.: +86 20 8529 0119; fax: +86 20 8529 0130.

E-mail addresses: longxp@gig.ac.cn (X. Long), yuanchao@gig.ac.cn (C. Yuan).

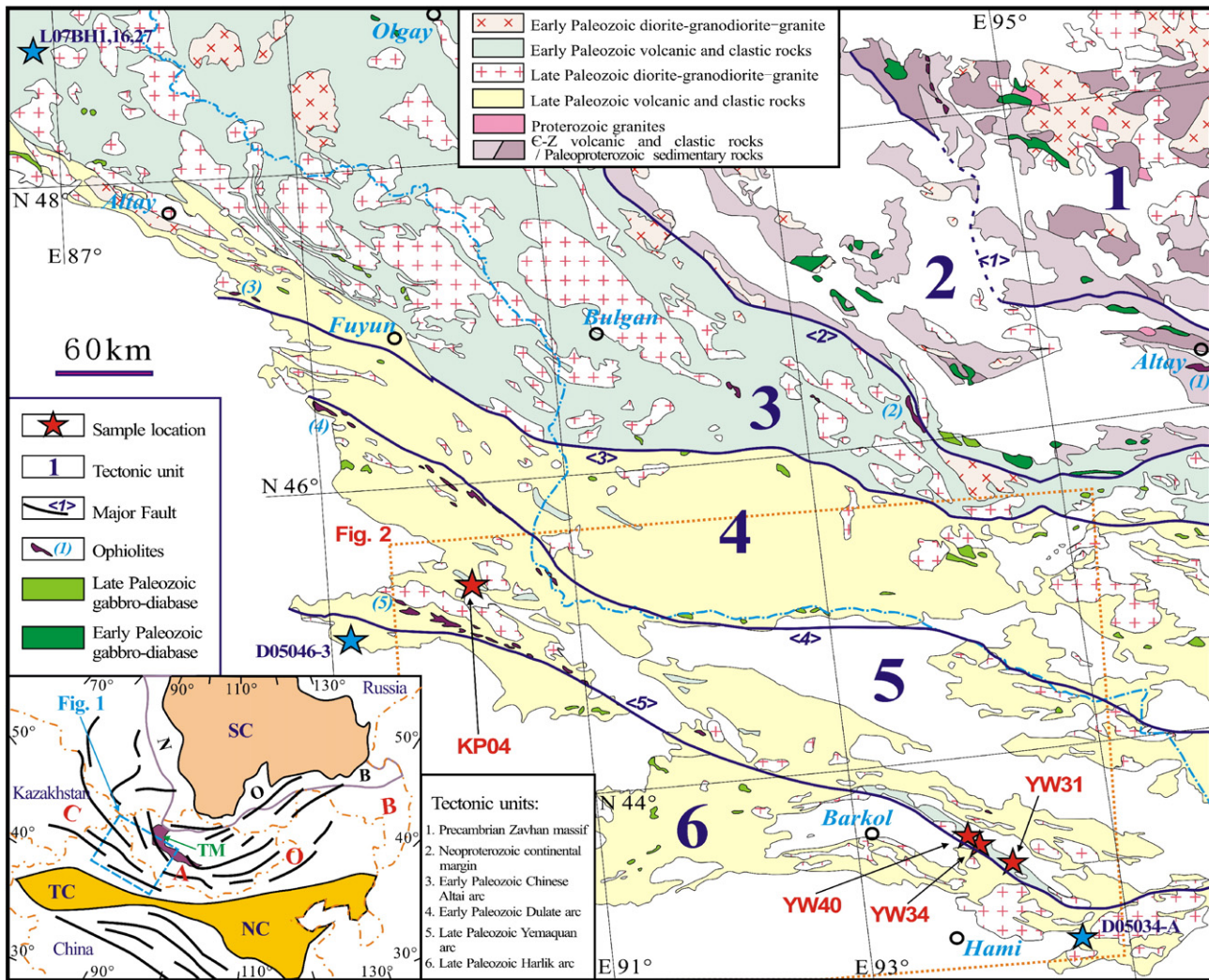


Fig. 1. Simplified geological map of the southern Central Asian Orogenic Belt (after He, 2004). Major faults: 1 Altay–Zavhan Fault; 2 Hovd Fault; 3 Erqis Fault; 4 Armantai Fault; 5 Kalamaili Fault. Ophiolites: 1 Altay ophiolite; 2 Bulgan ophiolite; 3 Kuerti ophiolite; 4 Armantai ophiolite; 5 Kalamaili ophiolite. Inset shows a simplified tectonic map of the Central Asian Orogenic Belt (Jahn et al., 2000). Abbreviations: SC, Siberian Craton; NC, North China Craton; TC, Tarim Craton; CAOB, Central Asian Orogenic Belt; NOB, Neoproterozoic Orogenic Belt; TM, Tuva–Mongolian Massif. Sample locations are marked with stars: red color for this study and blue color for previous studies (Li et al., 2007; Long et al., 2007, 2010; Sun et al., 2007).

regional tectonic evolution (Nelson, 2001; Cullers and Podkovyrov, 2002; Griffin et al., 2004; Hofmann, 2005; Gerdes and Zeh, 2006; Dickinson and Gehrels, 2009; Safonova et al., 2010). Recently, such studies were successfully applied to terranes in the southern CAOB (Long et al., 2007, 2008, 2010; Kelty et al., 2008; Kröner et al., 2010; Ren et al., 2011; Rojas-Agramonte et al., 2011).

The Junggar Block is one of the largest terranes in the southern CAOB and is located between the Chinese Altai and Tianshan orogenic belts (Xiao et al., 2004, 2008; Fig. 1, inset B). It is traditionally divided into three parts: Junggar Basin, East Junggar and West Junggar (e.g. BGMRX 1993). The Junggar Basin is mainly filled with pre-Carboniferous marine and post-Carboniferous continental sediments, whereas the East and West Junggar are dominated by igneous rocks, which form the basin ranges (BGMRX 1993; Zhang et al., 2009). Based on gravitational, aeromagnetic and seismic data, it has been suggested that the basin is underlain by ancient continental basement and that the Junggar Block was a Precambrian microcontinent (e.g. Li, 2004; Charvet et al., 2007, and references therein). However, based on the geochemical and Nd juvenile isotopic features of igneous rocks surrounding the Junggar Basin, other authors have interpreted the

Junggar block as a fragment of accreted oceanic crust and/or a volcanic arc of Early Paleozoic age (Filippova et al., 2001; Chen and Jahn, 2004; Jahn, 2004; Long et al., 2006; Yuan et al., 2006; Zheng et al., 2007; Xiao et al., 2008). In addition, the suture zone that stitches the Siberian plate to the Tarim plate, and to which plate the Junggar Block belongs has been a subject of debate for the past several years (e.g., Xiao et al., 1990; Ma et al., 1997; Shu et al., 2000). The occurrence of ophiolitic terranes of various ages around the Junggar Basin (i.e., in East and West Junggar) is also indicative of a complex history for the southern and resulted in many, often controversial, regional tectonic reconstructions (Jian et al., 2003; Ping et al., 2005; Tang et al., 2007; Xiao et al., 2008, 2009; Wang et al., 2009).

In this paper, we present new geochemical and geochronological data on Paleozoic graywackes from the lower sedimentary units of East Junggar (Fig. 1). Our results provide new constraints on the provenance of the graywackes and their depositional tectonic settings, which are indicative of Paleozoic subduction–accretion processes in East Junggar. The data also contribute to our understanding of the complex tectonic evolution of the Junggar Block and that of the southern CAOB.

2. Geological setting

East Junggar is located between the Early Paleozoic Chinese Altai magmatic arc and the Late Paleozoic Harlik arc, which are separated by the Erqis accretionary complex to the north and the Kalamaili ophiolite belt to the south (Fig. 1; Li, 2004; Xiao et al., 2008). The East Junggar terrane is dominated by Paleozoic accretionary complexes formed during northward subduction of the southern Paleo-Asian Ocean (PAO) (Coleman, 1989; Feng et al., 1989; Şengör and Natal'in, 1996; Xiao et al., 2009; Xiao et al., 2011). It is made up of the NW-striking Dulate and Yemaquan island-arcs, which are separated by the highly deformed and dismembered Armantai ophiolite belt (Fig. 2; Li, 2003; Xiao et al., 2004). The Dulate arc extends along the northern side of the Armantai ophiolite and consists mainly of Devonian–Carboniferous volcanic rocks, including picrite, boninite, high-Mg andesite, and Nb-rich basalt (Zhang et al., 2005; Zhang et al., 2008). The Yemaquan arc is located south of the Armantai ophiolite and is dominated by Ordovician–Carboniferous clastic rocks and carbonates, with subordinate volcanoclastic rocks (BGMRX, 1993; Xiao et al., 2009).

SHRIMP U–Pb zircon dating of the ophiolite belts in East Junggar yielded Early Paleozoic ages of 481 ± 5 to 489 ± 4 and 503 ± 7 Ma for the Armantai ophiolite (Jian et al., 2003; Xiao et al., 2008, 2009), and Middle–Late Paleozoic ages of 403 ± 9 to 330 ± 2 Ma for the Kalamaili ophiolite (Ping et al., 2005; Tang et al., 2007; Wang et al., 2009). According to the reconstructions by Xiao et al. (2009), the Armantai and Kalamaili ophiolites were formed by subduction of the southern branch of the PAO during the Early to Middle Paleozoic. The presence of uniformly deposited Late Carboniferous continental volcanic-sedimentary sequences on both sides of the Armantai ophiolite belt allowed Li (2004) to suggest that closure of the PAO in East Junggar predated the Late Carboniferous and was followed by post-collisional

A-type granitoids and Cu–Ni-bearing mafic and ultramafic plutons (Han et al., 2006; Mao et al., 2008; Zhang et al., 2008). Recent geochronological studies demonstrate that the post-collisional plutons intruded during the Late Carboniferous to the Permian, within an age span of 280–330 Ma (Li et al., 2004; Lin et al., 2007; Tang et al., 2007; Mao et al., 2008; Su et al., 2008; Yang et al., 2008, 2009; Chen et al., 2009).

Early Paleozoic sediments in East Junggar are mainly exposed in the Yemaquan arc terrane. The oldest sedimentary stratum, the Middle–Late Ordovician Huangcaopo Group (HG), consists of low-grade marine clastic sediments and andesitic–felsic volcanic rocks (BGMRX, 1993). The group occurs in the southeastern Yemaquan arc and has been divided into (from bottom to top), the Wuliegai, Daliugou and Miaoergou formations (Cai, 1999). The Wuliegai and Miaoergou formations are mainly composed of tuffaceous and calcareous sandstone and siltstone, intercalated with minor limestones, whereas the Daliugou formation comprises andesitic–felsic volcanic rocks, interlayered with subordinate tuffs and siltstones. The Middle to Late Silurian Kubusu Group (KG) and Hongliuxia Formation, which unconformably overlie the HG, occur mainly in the Yemaquan arc and are dominated by marine siltstone and sandstone (BGMRX, 1993). The Late Paleozoic sedimentary sequences in East Junggar consist of Devonian to Carboniferous arc-related volcanic rocks and clastic sediments, which are widely distributed in both the Dulate and Yemaquan arc terranes (Zhang et al., 2009).

Fresh graywackes from the HG and KG were sampled for geochemistry and detrital zircon U–Pb dating (Fig. 1). All samples consist of subangular to subrounded, moderately to poorly sorted grains of quartz (10–20%), feldspar (20–30%) and rock fragments (15–25%) within a silt-clay matrix. The rock fragments consist of andesitic to felsic volcanic rocks and less abundant slightly metamorphosed

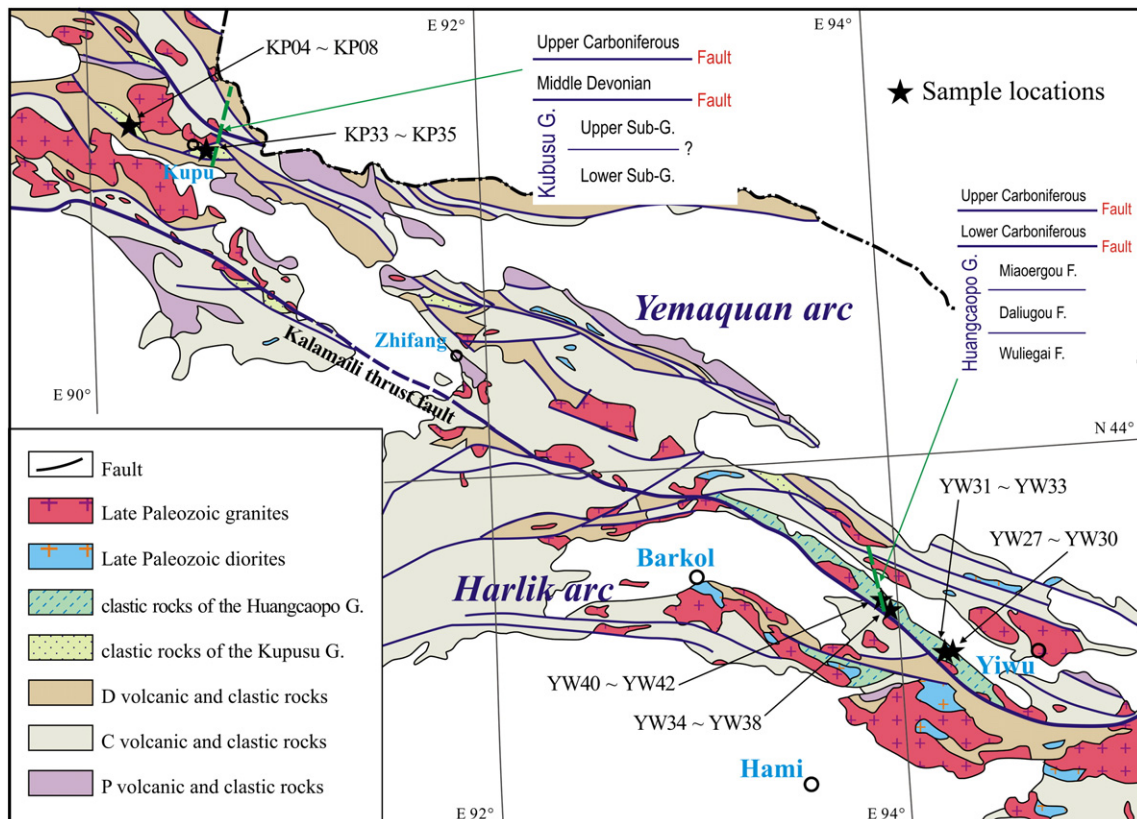


Fig. 2. Geological map of East Junggar with sample locations (after BGMRX, 1993).

Table 1
Geochemical compositions of graywackes from the Huangcaopo Group and Kubusu Group.

Sample strata	YW27	YW28	YW29	YW30	YW33	YW35	YW36	YW37	YW38	YW41	YW42	Average
Huangcaopo Group (HG)												
<i>Major element (wt.%)</i>												
SiO ₂	63.4	64.1	62.7	63.7	88.3	67.7	67.2	66.7	49.6	68.0	61.1	65.7
TiO ₂	0.73	0.69	0.78	0.78	0.18	0.58	0.62	0.66	1.29	0.79	0.87	0.7
Al ₂ O ₃	16.7	16.5	16.3	16.1	5.3	14.8	14.9	14.9	17.8	16.2	18.5	15.3
Fe ₂ O ₃ ^I	5.86	5.56	6.52	6.35	0.98	5.03	5.11	5.20	11.17	4.05	4.57	5.5
MnO	0.07	0.07	0.11	0.10	0.04	0.09	0.09	0.10	0.18	0.05	0.10	0.1
MgO	3.23	2.93	3.36	3.31	0.05	2.20	2.48	2.63	5.07	1.08	1.31	2.5
CaO	0.22	0.50	1.44	1.26	0.74	2.34	2.54	2.72	6.94	0.40	1.27	1.9
Na ₂ O	2.10	1.54	2.08	2.07	1.92	3.22	3.28	3.32	3.73	4.02	5.73	3.0
K ₂ O	4.29	4.70	2.87	2.80	1.03	2.19	2.05	1.87	0.61	2.64	3.86	2.6
P ₂ O ₅	0.11	0.10	0.22	0.21	0.05	0.17	0.18	0.20	0.18	0.14	0.26	0.2
LOI	3.09	3.38	3.40	3.13	0.98	1.45	1.42	1.32	3.33	2.42	2.19	2.4
Total	99.8	100.1	99.8	99.8	99.6	99.7	99.8	99.7	99.9	99.8	99.8	99.8
<i>Trace element (ppm)</i>												
Sc	14.4	14.9	15.7	15.8	1.79	10.4	17.0	9.4	20.1	15.7	13.8	13.5
Cr	88.7	86.7	85.9	97.5	11.6	66.6	99.5	88.6	15.2	31.5	26.8	63.5
Co	9.03	5.01	23.11	11.84	0.52	12.51	17.20	15.12	44.56	2.85	8.38	13.6
Ni	34.57	34.56	50.33	49.31	3.68	33.04	55.33	37.08	14.68	11.55	9.45	30.3
Ga	22	21	21	20	5	18	21	18	22	19	22	18.9
Rb	193	243	179	170	42	119	205	101	65	97	53	133.2
Sr	48	49	195	189	47	309	157	314	1860	250	252	333.4
Ba	494	637	424	399	243	339	575	232	121	577	243	389.3
Y	26	32	37	37	12	33	30	37	33	38	40	32.2
Zr	196	200	214	211	103	190	202	244	123	268	301	204.5
Nb	10.7	10.6	9.85	10.0	2.96	8.29	10.1	9.93	3.04	10.4	10.0	8.7
Hf	5.13	5.28	5.18	4.95	2.39	4.44	4.85	5.65	2.84	6.10	6.51	4.8
Ta	0.88	0.86	0.80	0.80	0.30	0.67	0.80	0.81	0.21	0.75	0.67	0.7
Pb	11.2	13.0	18.1	10.4	11.7	11.9	13.1	22.1	5.48	15.9	6.44	12.7
Th	12.4	12.8	12.0	11.9	6.58	9.61	12.9	12.3	2.25	7.90	4.29	9.5
U	3.23	2.44	2.71	2.54	1.36	2.18	2.35	2.76	0.83	2.23	1.68	2.2
La	27.2	29.8	33.0	27.0	24.3	27.2	30.5	29.1	9.0	25.2	25.9	26.2
Ce	58.6	65.3	70.4	64.0	46.8	57.4	62.7	68.9	23.7	56.3	59.1	57.5
Pr	6.97	7.97	8.86	7.53	5.37	7.10	7.56	8.39	3.55	7.11	7.59	7.1
Nd	27.1	32.0	35.4	30.1	20.8	28.5	29.1	34.9	16.7	28.7	32.8	28.7
Sm	5.28	6.11	7.10	6.31	3.11	5.69	5.53	7.06	4.50	5.98	6.84	5.8
Eu	1.15	0.99	1.48	1.42	0.76	1.29	1.24	1.39	1.52	1.34	1.49	1.3
Gd	4.80	5.34	6.53	6.15	2.59	5.52	5.20	6.45	4.83	5.70	6.30	5.4
Tb	0.76	0.89	1.05	1.03	0.36	0.89	0.84	1.07	0.85	1.00	1.05	0.9
Dy	4.32	5.04	6.08	6.05	1.89	5.20	4.72	5.90	5.06	6.09	6.06	5.1
Ho	0.90	1.08	1.23	1.26	0.37	1.05	0.96	1.17	1.06	1.31	1.29	1.1
Er	2.63	3.05	3.50	3.46	1.01	2.93	2.79	3.43	2.85	3.73	3.69	3.0
Tm	0.41	0.47	0.51	0.52	0.15	0.44	0.43	0.51	0.42	0.57	0.57	0.5
Yb	2.68	3.20	3.45	3.36	1.02	2.89	2.81	3.40	2.69	3.81	3.74	3.0
Lu	0.43	0.51	0.54	0.54	0.16	0.47	0.46	0.55	0.43	0.61	0.61	0.5
ClA	66	66	64	65	49	55	55	55	48	61	54	57.9
PIA	76	77	69	70	48	57	56	55	48	64	55	61.3
ICV	0.99	0.97	1.05	1.04	0.93	1.06	1.09	1.11	1.63	0.81	0.96	1.1
La _N /Yb _N	7.30	6.69	6.86	5.76	17.05	6.75	7.80	6.14	2.41	4.74	4.97	7.0
Gd _N /Yb _N	1.48	1.38	1.56	1.52	2.10	1.58	1.53	1.57	1.48	1.24	1.39	1.5
Eu/Eu*	0.69	0.52	0.65	0.69	0.79	0.69	0.70	0.62	0.99	0.69	0.68	0.7
ΣREE	143	162	179	159	109	146	155	172	77	147	157	146
Sample strata	Kubusu Group (KG)											
	KP02	KP03	KP05	KP06	KP07	KP08	KP33	KP34	KP35	Average	PAAS	
<i>Major element (wt.%)</i>												
SiO ₂	73.5	72.0	64.7	62.5	71.1	73.1	49.8	66.4	67.2	66.7	62.8	
TiO ₂	0.48	0.51	0.75	0.81	0.60	0.30	1.17	0.81	0.67	0.7	1.00	
Al ₂ O ₃	12.1	13.1	17.4	17.5	14.3	13.6	15.7	14.6	14.6	14.8	18.9	
Fe ₂ O ₃ ^I	3.27	3.57	5.41	4.31	2.53	2.74	8.08	5.47	4.73	4.5	6.50	
MnO	0.12	0.10	0.09	0.09	0.08	0.06	0.12	0.12	0.11	0.1	0.11	
MgO	1.01	1.07	1.63	1.21	0.77	1.00	8.41	1.79	1.57	2.1	2.20	
CaO	1.67	1.38	0.55	2.02	1.53	0.90	6.36	1.99	2.33	2.1	1.30	
Na ₂ O	3.78	5.47	5.97	6.04	5.59	6.37	3.44	4.50	5.70	5.2	1.20	
K ₂ O	1.95	0.98	1.48	2.96	1.87	0.42	1.45	1.84	0.71	1.5	3.70	
P ₂ O ₅	0.11	0.10	0.15	0.27	0.19	0.09	0.28	0.21	0.18	0.2	0.16	
LOI	1.79	1.42	1.58	2.00	1.08	1.12	5.20	1.99	2.01	2.0	-	
Total	99.7	99.7	99.7	99.8	99.7	99.7	100.1	99.7	99.7	99.8	97.9	
<i>Trace element (ppm)</i>												
Sc	8.40	7.69	15.0	10.6	9.36	2.57	21.9	13.0	11.0	11.1	16.0	
Cr	9.09	8.62	10.5	8.99	7.08	7.57	333	7.47	11.7	44.8	110	
Co	3.38	2.19	5.95	9.87	2.08	1.04	34.02	6.16	6.38	7.9	23	

Table 1 (continued)

Sample strata	KP02	KP03	KP05	KP06	KP07	KP08	KP33	KP34	KP35	Average	PAAS
	Kubusu Group (KG)										
Trace element (ppm)											
Ni	6.32	5.71	5.14	5.33	4.00	4.14	197	5.07	5.51	26.5	55
Ga	12	11	18	16	13	11	17	18	15	14.7	20
Rb	34	15	87	32	32	6	36	23	6	30.0	160
Sr	173	299	650	452	340	290	441	351	325	368.8	200
Ba	694	316	1278	740	409	129	443	498	143	516.5	650
Y	21	24	25	21	22	7	23	36	37	24.1	27
Zr	151	190	155	146	154	101	156	213	217	164.7	210
Nb	5.58	5.91	5.74	5.40	6.28	4.10	5.44	5.14	5.19	5.4	19.0
Hf	4.61	5.62	4.68	4.20	4.40	3.26	4.24	6.36	6.24	4.8	5.00
Ta	0.47	0.44	0.43	0.39	0.49	0.40	0.40	0.40	0.42	0.4	1.28
Pb	15.0	12.0	7.28	8.88	11.2	8.46	3.94	8.26	7.84	9.2	20.0
Th	4.46	5.89	6.33	4.72	4.73	5.09	2.52	2.75	3.01	4.4	14.6
U	1.75	2.35	2.17	2.01	1.98	2.04	0.73	1.20	1.33	1.7	3.10
La	12.0	16.2	20.1	16.2	18.5	11.9	18.1	15.1	12.4	15.6	38.2
Ce	27.8	36.3	41.4	35.9	39.5	23.8	41.4	36.8	31.3	34.9	79.6
Pr	3.82	4.57	5.25	4.32	5.23	2.77	5.74	4.98	4.43	4.6	8.83
Nd	16.0	19.1	22.2	17.9	21.8	10.0	24.7	22.7	19.6	19.3	33.9
Sm	3.64	4.08	4.96	3.91	4.51	1.78	5.16	5.49	4.74	4.3	5.55
Eu	0.83	0.85	1.41	1.08	1.09	0.37	1.63	1.45	1.00	1.1	1.08
Gd	3.58	4.00	4.89	3.89	4.14	1.52	4.93	5.64	5.28	4.2	4.66
Tb	0.65	0.71	0.79	0.63	0.70	0.24	0.80	1.04	1.00	0.7	0.77
Dy	3.95	4.40	4.74	3.81	4.26	1.39	4.63	6.38	6.54	4.5	4.68
Ho	0.87	0.94	1.00	0.82	0.88	0.28	0.93	1.36	1.44	0.9	0.99
Er	2.45	2.73	2.75	2.39	2.53	0.81	2.52	4.00	4.31	2.7	2.85
Tm	0.40	0.44	0.43	0.38	0.40	0.12	0.37	0.61	0.69	0.4	0.41
Yb	2.65	2.90	2.83	2.49	2.69	0.84	2.29	3.99	4.56	2.8	2.82
Lu	0.42	0.47	0.44	0.40	0.42	0.13	0.34	0.63	0.74	0.4	0.43
CIA	52	51	58	51	51	52	45	53	50	51.4	69
PIA	52	51	59	51	51	52	45	53	50	51.7	77
ICV	1.01	1.00	0.91	1.00	0.90	0.87	1.85	1.13	1.09	1.1	0.85
La _N /Yb _N	3.25	4.01	5.09	4.67	4.92	10.19	5.69	2.71	1.95	4.7	9.72
Gd _N /Yb _N	1.12	1.14	1.43	1.29	1.27	1.50	1.78	1.17	0.96	1.3	1.37
Eu/Eu*	0.69	0.63	0.87	0.84	0.76	0.67	0.97	0.79	0.61	0.8	0.63
ΣREE	79	98	113	94	107	56	113	110	98	96	185

Note: CIA = $[\text{Al}_2\text{O}_3 / (\text{Al}_2\text{O}_3 + \text{CaO}^* + \text{Na}_2\text{O} + \text{K}_2\text{O})] \times 100$ and PIA = $[(\text{Al}_2\text{O}_3 - \text{K}_2\text{O}) / (\text{Al}_2\text{O}_3 + \text{CaO}^* + \text{Na}_2\text{O} - \text{K}_2\text{O})] \times 100$, where CaO* represents Ca in silicate-bearing minerals only and all in molecular proportions; ICV = $(\text{Fe}_2\text{O}_3 + \text{K}_2\text{O} + \text{Na}_2\text{O} + \text{CaO} + \text{MgO} + \text{TiO}_2) / \text{Al}_2\text{O}_3$; PAAS from Taylor and McLennan (1985).

sedimentary rocks, i.e., pelite and sandstone. The matrix (~30 vol.%) of the graywackes mainly consists of a matted mixture of tiny grains of quartz, feldspar and clay minerals with accessory chlorite and epidote.

3. Results

3.1. Geochemistry of graywackes

3.1.1. Major elements

The HG graywackes show a relatively narrow variation in SiO₂ content from 61.1 wt.% to 68.0 wt.%, with an average of 65.7 wt.%. The samples have wide ranges of Na₂O (1.54–5.73 wt.%, av. 3.04 wt.%) and K₂O (1.87–4.70 wt.%, av. 3.03 wt.%), with Na₂O/K₂O ratios between 0.3 and 1.8. In comparison with the Post-Archean Australian average shale (PAAS) (Taylor and McLennan, 1985), the HG samples yield lower Al₂O₃ (av. 16.1 wt.%) and Fe₂O₃^T (av. 5.36 wt.%) and higher MgO (av. 2.50 wt.%), implying a more mafic source. Although the HG and KG graywackes have similar mineral/lithic assemblages, they exhibit clear geochemical differences (Table 1). The KG graywackes show a relatively wide variation in SiO₂ (62.5–73.5 wt.%) and much lower Al₂O₃ (av. 14.7 wt.%), Fe₂O₃^T (av. 4.00 wt.%), MgO (av. 1.26 wt.%) and K₂O (av. 1.53 wt.%), and higher Na₂O (av. 5.43 wt.%). All HG and KG samples are characterized by negative correlations between TiO₂, Al₂O₃ and Fe₂O₃^T versus SiO₂, but there is no correlation between Na₂O and K₂O versus SiO₂ (Fig. 3).

3.1.2. Trace elements

The sampled graywackes show positive correlations in the K₂O versus Ba and K₂O versus Rb diagrams (Fig. 4a, b). These correlations suggest that K-bearing clay minerals (e.g., illite, kaolinite) control the abundances of Ba, K and Rb in the graywackes (McLennan et al., 1983). No clear trends are observed in the K₂O versus Sr plot (Fig. 4c). The KG samples have higher Sr than the HG samples (Table 1), implying intensified plagioclase fractionation in the source.

Cr and Ni are well correlated in the graywackes (Fig. 4), suggesting no fractionation between them during weathering (Feng and Kerrich, 1990). Compared with the average composition of the upper continental crust, the HG and KG samples have respectively higher Cr and lower Ni abundances. The increase of Cr, Ni and MgO in the HG versus KG sediments confirms that the HG sediments were derived from a more mafic source. Unlike Cr, Ni and MgO, the High Field Strength Elements (HFSE, e.g., Zr, Hf, Nb, Ta, Th, U) are usually abundant in felsic rocks and, therefore, we would expect a lower abundance in the HG compared to the KG samples. However, the HG samples exhibit slightly higher HFSEs than the KG samples. Because the HFSEs are usually abundant in accessory minerals (e.g. rutile and zircon), we suggest that the slightly higher HFSEs in the HG samples indicate a greater abundance of accessory minerals in the source of the HG compared to the KG.

All rock samples are enriched in light Rare Earth Element (REE) and show relatively horizontal heavy REE patterns (La_N/Yb_N = 1.95–10.2, Fig. 5). Although the HG samples have higher La_N/Yb_N ratios (av. 6.33) than those of the KG samples (La_N/Yb_N av. = 4.60), they all show similar moderate negative Eu anomalies (HG: Eu/Eu*_{av.} = 0.66;

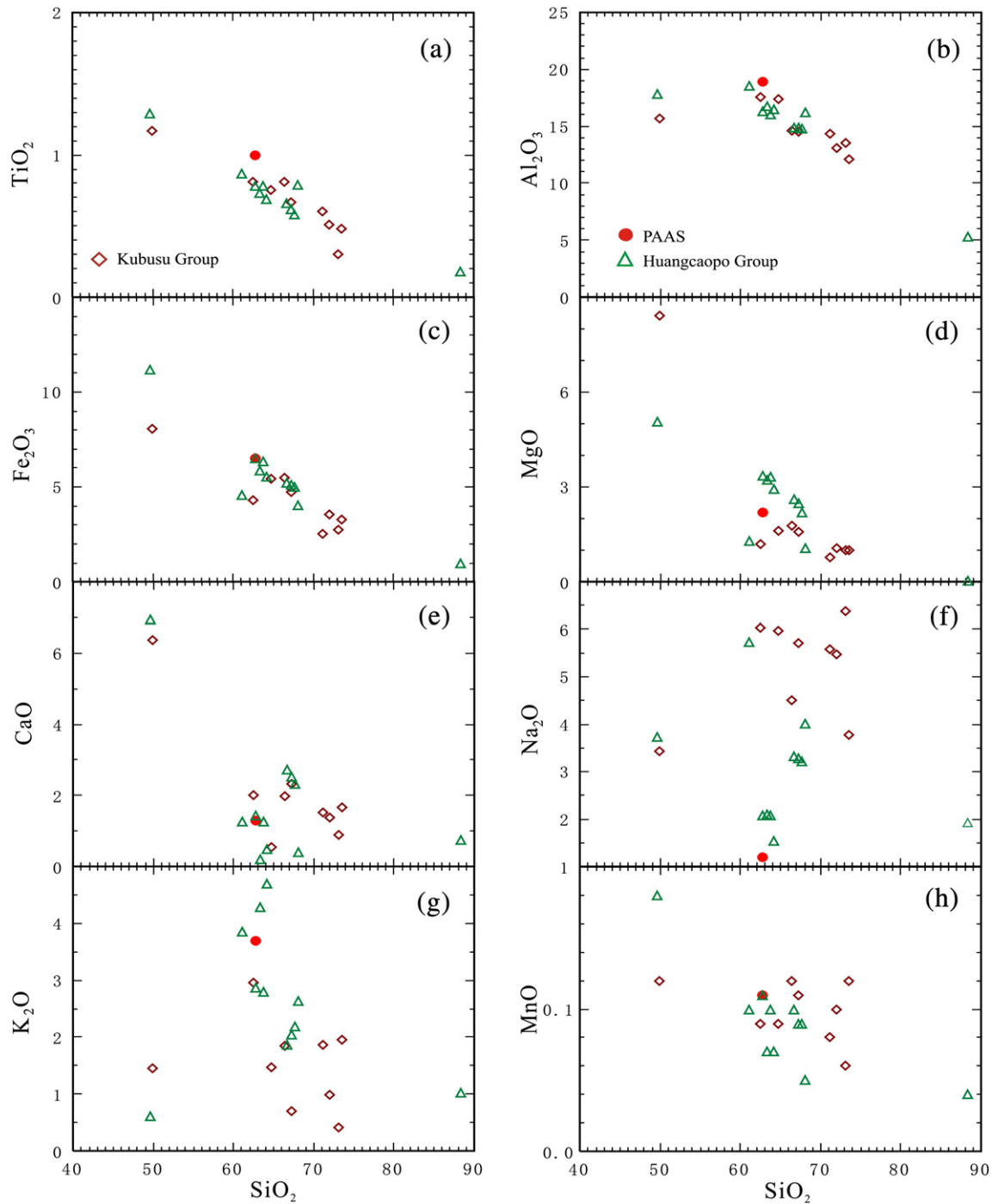


Fig. 3. Geochemical diagrams of major elements for the Paleozoic graywackes in East Junggar. Data for PAAS are from Taylor and McLennan (1985).

KG: $\text{Eu}/\text{Eu}_{\text{av}}^* = 0.73$), resembling PAAS ($\text{Eu}/\text{Eu}_{\text{av}}^* = 0.65$, Taylor and McLennan, 1985). Both graywackes display REE patterns and spider diagrams similar to the Habahé flysch sediments in the neighboring Chinese Altai, which are thought to have been deposited in a fore-arc setting (Fig. 5; Long et al., 2008, 2010).

3.2. Detrital zircon U–Pb dating

3.2.1. Huangcaopo Group

Zircons in samples of the HG are 70 to 140 μm in size, transparent, mostly euhedral prismatic or, to a lesser degree, (sub)rounded. The zircons possess clear oscillatory zoning and high Th/U ratios (mostly

>0.2 , Fig. 6f), suggesting an igneous origin. Three samples were dated (Fig. 6a–c) and two of them (YW31 and YW34) yielded similar age spectra (Fig. 7a–b). In these two samples, prismatic zircons yielded Early Paleozoic $^{206}\text{Pb}/^{238}\text{U}$ ages, which exhibit a prominent age peak at ~ 490 Ma and a younger age peak at ~ 440 Ma. The remaining (sub) rounded zircons yielded various Precambrian ages (Supplementary Table A1), with the main age peak in the Neoproterozoic (~ 930 Ma, Fig. 7a–c). Five Paleoproterozoic $^{207}\text{Pb}/^{206}\text{Pb}$ ages (1.77–2.03 Ga) were identified in sample YW31 (Fig. 7a).

Zircons from the third sample (YW40) exhibit much younger $^{206}\text{Pb}/^{238}\text{U}$ ages (Fig. 6d). The prismatic zircons yielded Carboniferous to Cambrian ages, with two prominent age peaks: Early Carboniferous

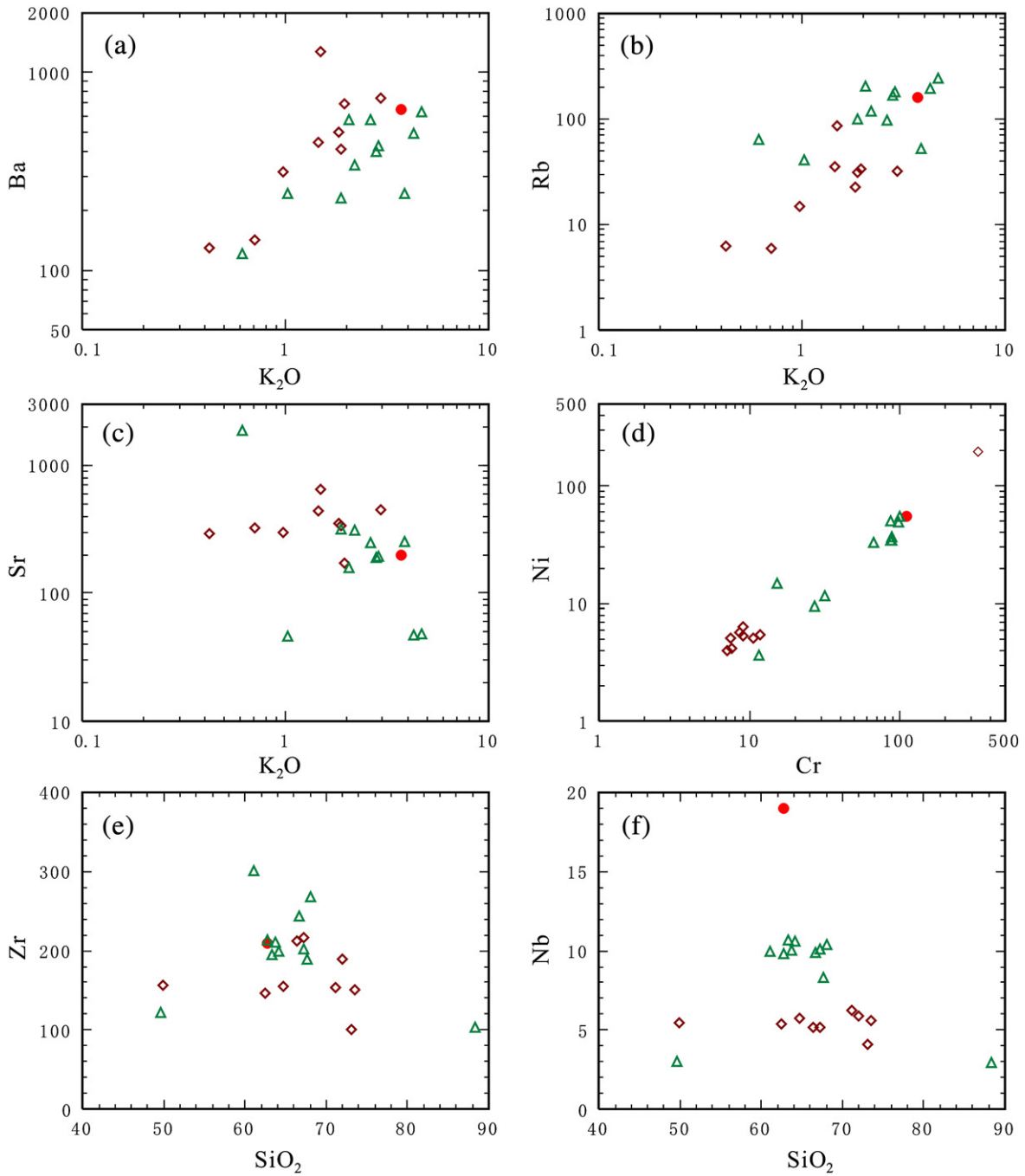


Fig. 4. Diagrams of geochemical compositions for the Paleozoic graywackes in the East Junggar. Symbols are as in Fig. 3. Data for PAAS are from Taylor and McLennan (1985).

(~353 Ma) and Early Silurian (~443 Ma). The latter age peak is similar to the younger age peak in the other two samples (YW31 and YW34) of the HG. The (sub)rounded zircons in sample YW40 also yielded Neoproterozoic ages, which fall into two age-groups with peaks at ~550 Ma and ~930 Ma (Fig. 7c). The ~930 Ma peak is also present in the age spectra of the other two samples of the HG group.

3.2.2. Kubusu Group

For the KG graywackes, only one sample (KP04) yielded sufficient dateable zircons. The zircons are very small (50 to 100 μm), transparent, and most of them are euhedral prismatic grains. All of the zircon grains possess clear oscillatory zoning and high Th/U ratios

(>0.48), indicating a source dominated by igneous rocks. U–Pb dating results for this sample yielded Early Carboniferous ²⁰⁶Pb/²³⁸U ages spanning a very narrow interval between 323 Ma and 395 Ma, with a clear peak at ~346 Ma that is similar to the youngest age peak in sample YW40 of the HG (Figs. 6e and 7d).

4. Constraints on depositional age

The depositional age of the Early Paleozoic sedimentary sequence in East Junggar is not well constrained due to the low abundance of dateable fossils (BGMRX, 1993). The HG was originally assigned to the middle–Late Ordovician (BGMRX, 1993). Later, the group was divided

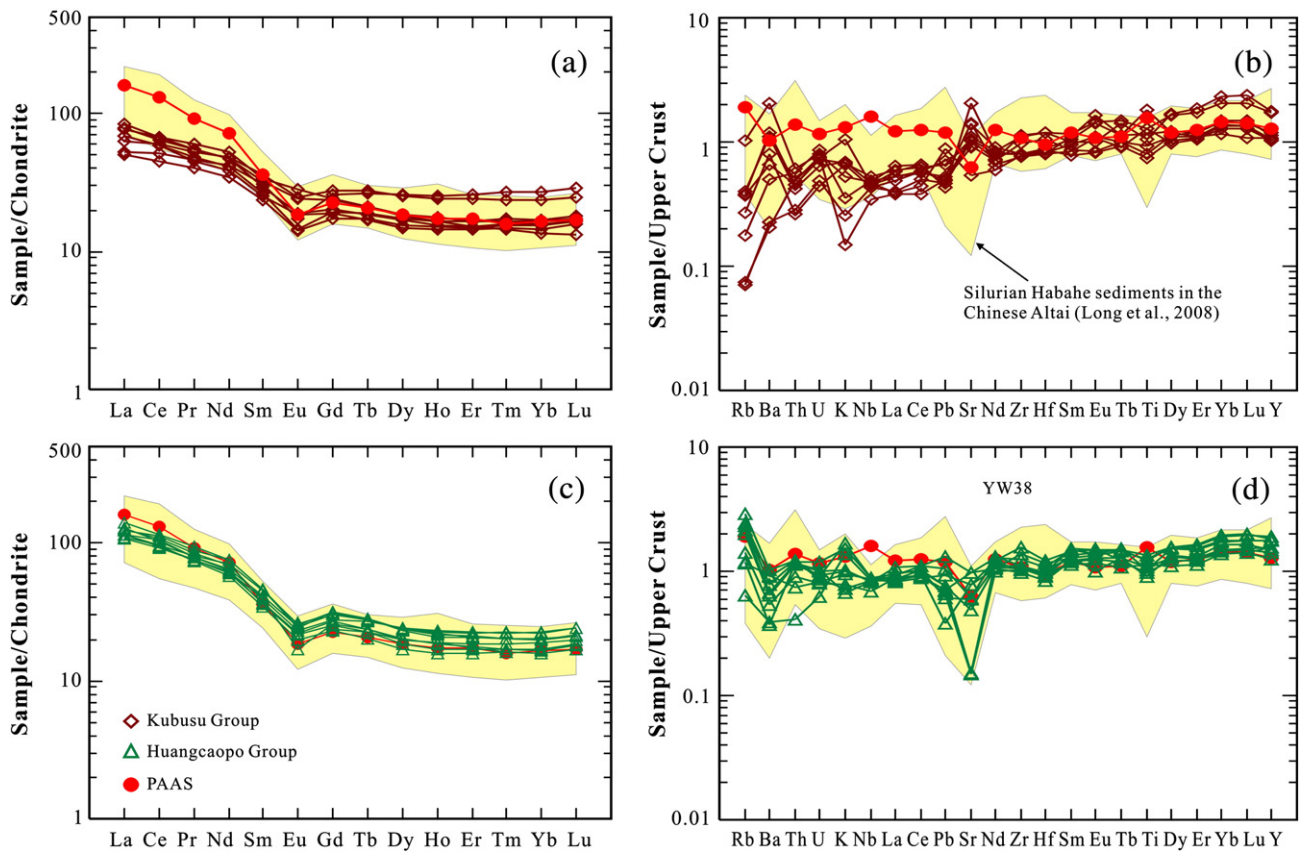


Fig. 5. Chondrite-normalized REE patterns and upper crust-normalized spider diagrams for the Paleozoic graywackes. Symbols are as in Fig. 3. Chondrite and PM normalizing values are from Sun and McDonough (1989) and upper crust-normalizing data are from Taylor and McLennan (1985).

into three formations (Fig. 2), but the depositional ages did not change (Cai, 1999). In this study, samples YW31 and YW34 were collected from the lowest subdivision of the HG, the Wuliegai Formation. The youngest zircon population in both samples gave Early Paleozoic $^{206}\text{Pb}/^{238}\text{U}$ ages of ~440 Ma, indicative of a post-Early Silurian depositional age for the Wuliegai Formation. Sample YW40 was collected from the uppermost subdivision, the Miaoergou Formation. The youngest $^{206}\text{Pb}/^{238}\text{U}$ age population in this sample peaks at ~355 Ma, suggesting a younger post-Early Carboniferous depositional age for the Miaoergou Formation. The most abundant age population of detrital zircons in YW40 spans the interval 335–400 Ma. However, no zircons with these ages have been identified in the stratigraphically older Wuliegai Formation. If the Wuliegai Formation was deposited after the Early Devonian (<400 Ma), the Devonian detrital zircons found in the Miaoergou Formation should also be present in the Wuliegai Formation. The absence of such zircons suggests that the Wuliegai Formation was deposited during the period from the Silurian to the Early Devonian (400–440 Ma). Therefore, depositional age of the HG may be younger than previously thought.

The graywackes of the KG are thrust onto Devonian strata within the study area and were previously considered to be part of the Middle to Late Silurian Hongliuxia Formation (BGMRX, 1993). However, all of the $^{206}\text{Pb}/^{238}\text{U}$ ages of the analyzed zircons in sample KP04 cluster around a single age peak at ~346 Ma. This suggests a younger depositional age for the KG graywackes and a source that was dominated by Early Carboniferous igneous rocks. Given that both the KG and the Miaoergou Formation have similar rock assemblages to those of the Early Carboniferous Nanmingshui Formation in this area (BGMRX, 1993) and have Carboniferous depositional ages, we suggest that the two sequences should be regarded as a part of the

Nanmingshui Formation. Therefore, the HG used in the following discussion does not include the Miaoergou Formation.

5. Discussion

5.1. Weathering characteristics

The Chemical Index of Alteration (CIA), the Plagioclase Index of Alteration (PIA) and the Index of Compositional Variability (ICV) are frequently used parameters of the weathering characteristics and source composition of sedimentary rocks (McLennan et al., 1993; Cox et al., 1995; Fedo et al., 1995; Cullers and Podkovyrov, 2000; Bhat and Ghosh, 2001). The graywackes in East Junggar have very low CIA values (50–66), indicating that they are not strongly weathered, or that compositionally mature alumina-rich minerals were absent in the source (Nesbitt and Young, 1982; Fedo et al., 1995). The CIA values of the KG samples (av. 52) are lower than those of the HG samples (av. 60), which suggest that the source of the KG graywackes was less weathered before deposition. More evidence can be found in their respective PIA values (KG samples: av. 51.7; HG samples: av. 61.3). In the ACNK (ACNK = molar ratio of $\text{Al}_2\text{O}_3/[\text{CaO} + \text{Na}_2\text{O} + \text{K}_2\text{O}]$) diagram (Fig. 8), the KG samples plot along the average gabbro-tonalite-granodiorite line, implying more fresh feldspars in the source, which had experienced no significant chemical weathering. The HG samples, however, plot away from the predicted weathering trend of gabbro-tonalite-granodiorite. This suggests that the HG graywackes were likely altered by post-depositional K-metasomatism. The identical average ICV values (~1.1) for both the KG and HG samples point to an immature source for the Paleozoic graywackes in East Junggar.

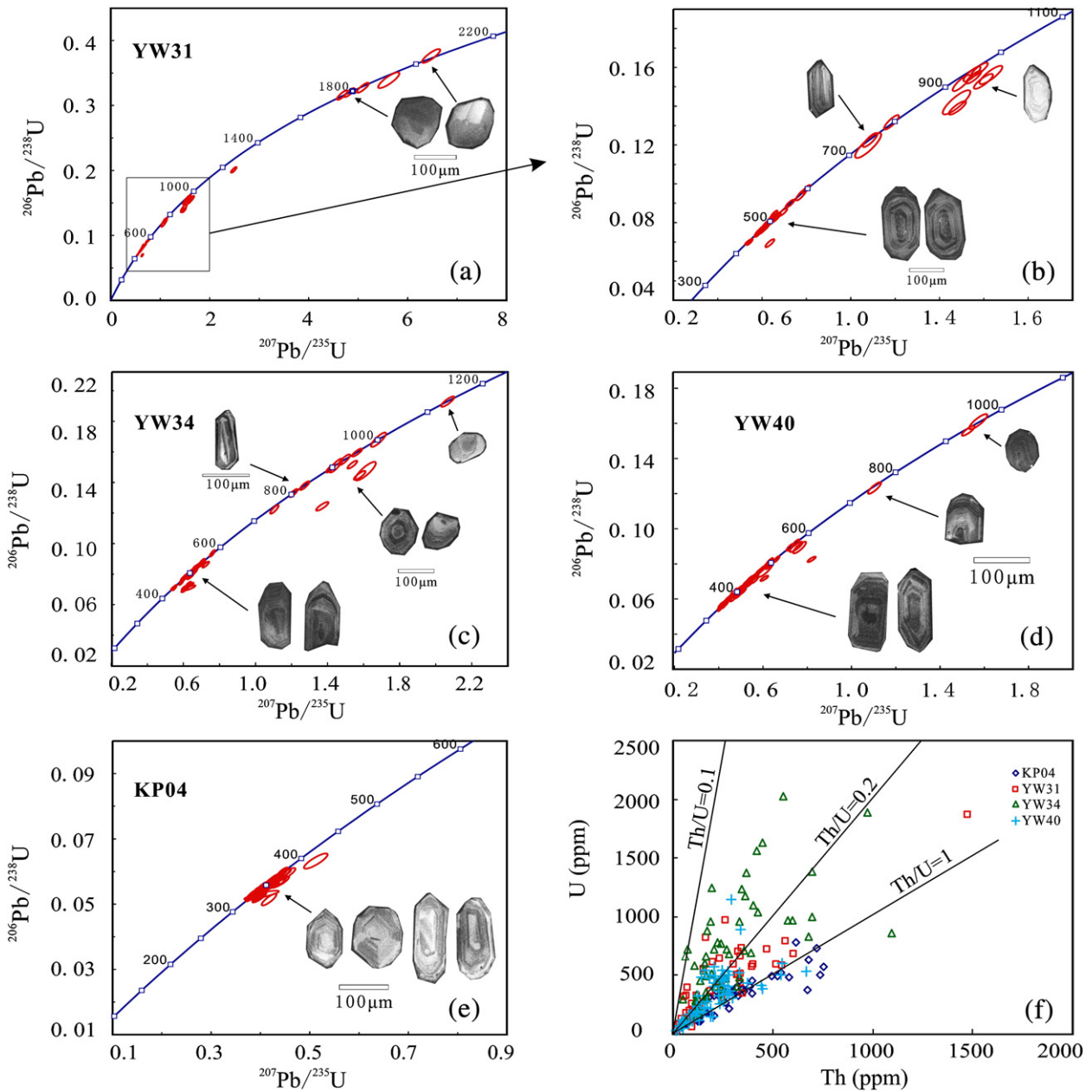


Fig. 6. U–Pb concordia diagrams and Th–U plots for detrital zircons from the Paleozoic graywackes with representative CL images.

The geochemistry of the graywackes and the large proportion of andesitic–felsic igneous rocks among the rock fragments suggest a magmatic arc source. All the graywackes show relatively wide variations of Th/Sc and a narrow range of Zr/Sc, which are positively correlated in the Th/Sc–Zr/Sc diagram (Fig. 9a). This reveals variable contributions of less reworked source material, which suggests that the provenance of the graywackes was controlled more by source composition than by sediment recycling (McLennan et al., 1993; Cullers, 1994). The graywackes were probably derived from a source dominated by felsic–andesitic igneous rocks that are marked by their low La/Th ratios and relatively high Hf contents (Fig. 9b).

5.2. Tectonic settings and provenance

The geochemistry of sediments deposited in oceanic island arc, continental island arc, active continental margin and passive margin tectonic settings, has been investigated by many researchers (e.g., Bhatia and Taylor, 1981; Bhatia and Crook, 1986; Roser and Korsch,

1986; McLennan et al., 1990; McLennan and Taylor 1991). Generally, Al_2O_3 , $Fe_2O_3^T + MgO$, TiO_2 and Al_2O_3/SiO_2 ratios decrease in sandstones from oceanic island arc settings to passive margins, while SiO_2 and K_2O/Na_2O ratios increase (Bhatia, 1983). The HG and KG samples have moderate SiO_2 , Al_2O_3 , TiO_2 and Al_2O_3/SiO_2 ratios that clearly differ from those of the graywackes formed in either setting. Instead, they show a strong affinity with graywackes from continental island arc or active continental margin settings (Table 2). The contents and ratios of trace elements (including REEs) in the HG and KG samples exhibit the greatest similarity to graywackes from continental island arcs (Table 2). In the discriminatory La–Th–Sc and Th–Sc–Zr/10 diagrams (Bhatia and Crook, 1986), most samples plot in continental arc field (Fig. 10a–b). Similar results are revealed by the Sc/Cr–La/Y and La/Sc–Ti/Zr diagrams (Bhatia and Crook, 1986) (Fig. 10c–d). These geochemical features, in combination with their weak weathering characteristics and immature source composition, suggest that the graywackes in East Junggar were deposited in a basin adjacent to a continental arc.

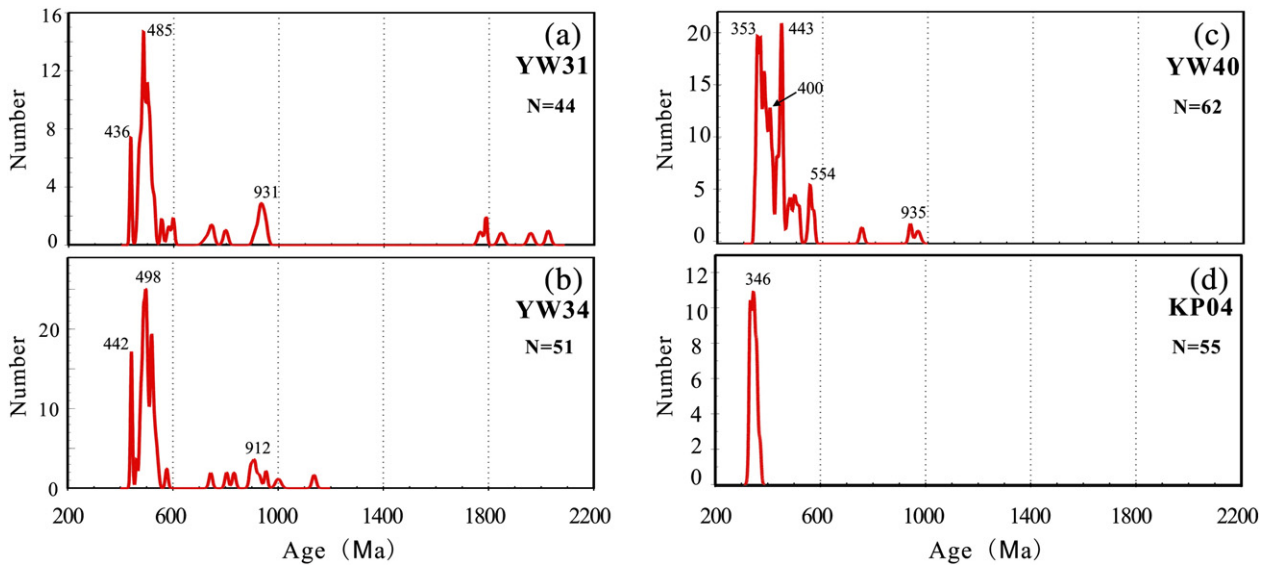


Fig. 7. Relative probability plots for detrital zircons from the Paleozoic graywackes ($^{206}\text{Pb}/^{238}\text{U}$ ages for zircons <1000 Ma and $^{207}\text{Pb}/^{206}\text{Pb}$ ages for zircons >1000 Ma).

The detrital zircon ages of the sampled graywackes can be grouped at ~350 Ma, ~440 Ma, ~500 Ma, 740–950 Ma, 1.7–2.0 Ga, and ~2.7 Ga (Fig. 7). Several recent studies have revealed that voluminous Late Devonian–Early Carboniferous volcanic rocks and granitoids are exposed in the Dulate arc (Zhang et al., 2006; Lin et al., 2008; Su et al., 2008; Tan et al., 2009), in the neighboring Chinese Altai (Wang et al., 2006; Tong et al., 2007; Yuan et al., 2007; Sun et al., 2009; Cai et al., 2010; Wang et al., 2010) and in South Mongolian arcs (Bibikova et al. 1992; Kozakov et al., 2002; Kröner et al., 2007; Yarmolyuk et al., 2008; Demoux et al., 2009a). The immature source and poorly sorted minerals and rock fragments of the graywackes suggest that one of the magmatic arcs could be the main source for the KG and the Miaoergou Formation. Early Paleozoic igneous rocks, especially ones older than 420 Ma, are sparse in East Junggar. However, ~440 and ~500 Ma igneous rocks are common in southern Mongolia (Bibikova et al. 1992; Kozakov et al., 2002; Kröner et al., 2007; Yarmolyuk et al., 2008; Demoux et al., 2009a) and in the

Chinese Altai (Wang et al., 2006; Yuan et al., 2007; Sun et al., 2008, 2009; Long et al., 2010). The older ages of 740–950 Ma, 1.7–2.0 Ga and ~2.7 Ga have been reported for the Tuva–Mongolian, Dzabkhan, Baga Bogd and South Gobi microcontinents (Kozakov et al., 1999, 2007; Kuzmichev, et al., 2001; Demoux et al., 2009b, 2009c). This suggests a potential source for the Precambrian materials of the graywackes. Precambrian rocks are also exposed in the Tarim and North China blocks, but their detrital zircon age distributions lack the age peaks at 500–700 Ma and 1.0–1.8 Ga (Gehrels and Yin, 2003; Darby and Gehrels, 2006). It is therefore unlikely that the two blocks supplied much clastic material to the graywackes of East Junggar (Fig. 11). Instead, we suggest that the Precambrian clastic material of the HG was derived from a source located to the north of East Junggar.

5.3. Evolution of the southern branch of the Paleo-Asian Ocean

Ophiolites represent remnants of oceanic crust, therefore, the presence of ophiolites in East Junggar is essential to our understanding of the Late Paleozoic evolution of the southern CAOB (Khain et al., 2002; Xiao et al., 2003, 2004; Windley et al., 2007). The Armantai and Kalamaili ophiolite belts are the largest ophiolites in East Junggar, which formed during the Paleozoic evolution of the southern PAO (Xiao et al., 2009). Recent zircon SHRIMP U–Pb dating of gabbros and a plagiogranite from the Armantai ophiolite yielded ages of 481 ± 5 to 489 ± 4 Ma (Jian et al., 2003) and 503 ± 7 Ma (Xiao et al., 2009), respectively, which indicate that the Armantai branch of the PAO was already open before the Early Ordovician. However, these ages do not provide close constraints on the closure of the Armantai Ocean. The occurrence of Ordovician and Middle–Late Devonian radiolarian cherts in the region suggests that the Armantai Ocean was still a wide ocean at that time and characterized by calm-water conditions (Li, 1991; Xiao and Tang, 1991, 1992; He et al., 2001). Based on the uniform Late Carboniferous continental volcanic–sedimentary rocks on the both sides of the Armantai ophiolite belt, Li (2004) suggested that closure of this oceanic branch predated the Late Carboniferous. Our detrital zircon age spectra for the Early Paleozoic HG (samples YW31 and YW34; Fig. 1) resemble that of the Habahe sediments in the Chinese Altai (Fig. 11). This suggests that no ocean or other geographical boundary existed between East Junggar and the Chinese Altai at the time the HG and Habahe sediments were deposited. Therefore, we suggest that the Armantai ophiolite was emplaced prior

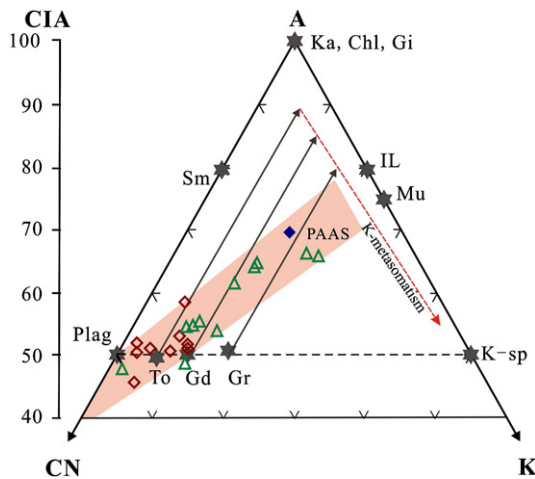


Fig. 8. ACNK diagram for the Paleozoic graywackes in East Junggar (after Fedo et al., 1995). CIA values range from 50 for fresh primary igneous rocks to a maximum of 100 for the most weathered rocks (Fedo et al., 1995). Arrows show the predicted weathering trend of To, Gd and Gr. Symbols are as in Fig. 3. Data for tonalite (To), granodiorite (Gd), granite (Gr) and average Archean upper crust are from Condie (1993).

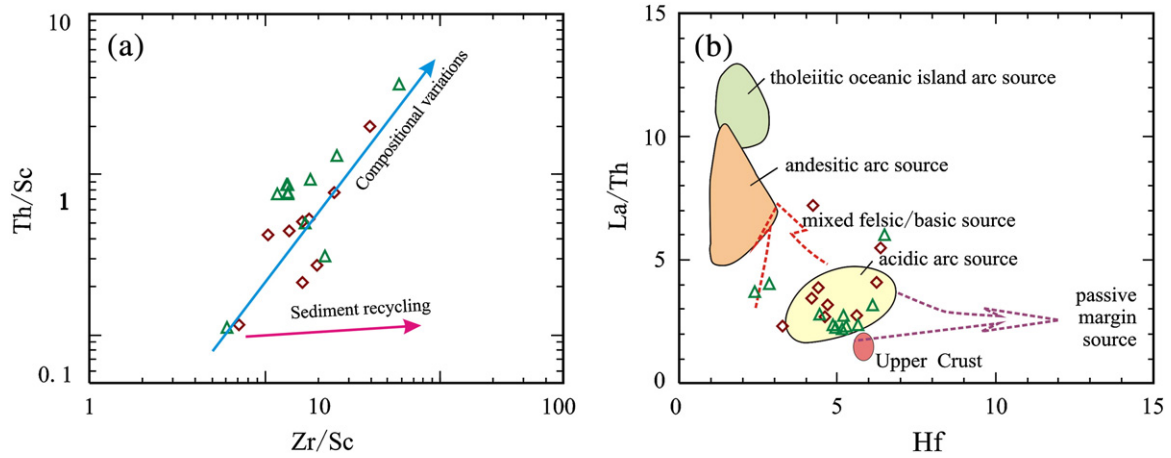


Fig. 9. Geochemical diagrams showing source variation and composition for the Paleozoic graywackes. Symbols are as in Fig. 3. (a) Zr/Sc–Th/Sc diagrams after McLennan et al. (1993); (b) La/Th–Hf diagram after Floyd and Leveridge (1987).

to oceanic closure and, hence, prior to the deposition of the HG and Habahe sediments. Since the HG and the Habahe sediments were deposited between the Silurian and Early Devonian, the emplacement of the Armantai ophiolite must at least predate the Early Devonian.

The Kalamaili ophiolite has been considered as the boundary between the East Junggar area and the Late Paleozoic Harlik arc (Li, 1995; Li et al., 2009). The Kalamaili tholeiitic gabbros and basalts possess island-arc affinities and plot in the fields of IAB and MORB in geochemical diagrams (Wang et al., 2003; Wang et al., 2009). Liang et al. (1999) suggested that the Kalamaili ophiolite formed in a fore-arc setting. Zircon SHRIMP U–Pb dating of plagiogranite and gabbros from the Kalamaili ophiolite yielded ages of 403 ± 9 , 336 ± 4 and 330 ± 2 Ma, suggesting that the southern branch of the PAO was already open in the Early Devonian (Ping et al., 2005; Tang et al., 2007; Wang et al., 2009). Recent U–Pb dating of detrital zircons from a Carboniferous sandstone sample on the south side of the ophiolite yielded major age peaks at 365, 403, 464 and 516 Ma, and scattered Neoproterozoic to Neoproterozoic ages (Li et al., 2007). The age distribution is characterized by relatively high percentages of zircons with Early Paleozoic ages (33%) and Precambrian ages (27%). This differs from the age spectra of detrital zircons from

sandstone samples of the Harlik arc, which are dominated by Early Paleozoic zircon ages (93%) (Sun et al., 2007). The detrital zircon age spectra of the Carboniferous samples in this study (YW40 and KP04) differ from both the Carboniferous sandstone in the southern Kalamaili ophiolite belt and the Carboniferous samples of the Harlik arc (Fig. 7). These differences suggest that an oceanic branch of the PAO may have persisted between East Junggar and the Harlik arc during the deposition of the KG and the Miaogou Formation (<350 Ma), which is consistent with the discovery of Late Devonian to Early Carboniferous radiolarian fossils in siliceous rocks in the Kalamaili ophiolite belt (Shu and Wang, 2003).

5.4. Tectonic implications for the southern CAOB

Many different models have been proposed to explain the tectonic evolution of the CAOB, including punctuated accretion by closure of multiple oceans (Coleman, 1989; Zonenshain et al., 1990), the formation of the Kipchak arc a single subduction zone (Şengör et al., 1993; Şengör and Natal'in, 1996), fore-arc accretion punctuated by opening and closure of back-arc basins (Yakubchuk et al., 2001, 2002), and collision

Table 2
Average chemical compositions of graywackes in East Junggar and graywackes in representative tectonic settings. Data for graywackes of various tectonic settings are from Bhatia (1983, 1985) and Bhatia and Crook (1986).

Tectonic setting					Huangcaopo G.		Kubusu G.	
	OIA	CIA	ACM	PM	Range	Average	Range	Average
Samples	Graywackes							
SiO ₂	59	71	74	82	61.1–68.0	65	62.5–73.5	68.8
TiO ₂	1.06	0.64	0.46	0.49	0.58–0.87	0.72	0.30–0.81	0.62
Al ₂ O ₃	17	14	13	8	14.8–18.5	16.1	12.1–17.5	14.7
Al ₂ O ₃ /SiO ₂	0.3	0.2	0.2	0.1	0.22–0.30	0.25	0.16–0.28	0.21
Ba	370	444	522	253	232–637	436	129–1278	526
Pb	7	15	24	16	6.44–22.1	13.6	7.28–15.0	9.87
Th	2	11	19	17	4.29–12.9	10.7	2.75–6.33	4.62
U	1	3	4	3	1.68–3.23	2.46	1.20–2.35	1.85
Zr	96	229	179	298	190–301	225	101–217	166
Hf	2.1	6.3	6.8	10.1	4.44–6.51	5.34	3.26–6.36	4.92
Nb	2.0	8.5	10.7	7.9	8.29–10.7	9.99	4.10–6.28	5.42
Nd	11	21	25	29	27.1–35.4	31.0	10.0–22.7	18.7
La _N /Yb _N	2.8	7.5	8.3	10.8	4.74–7.80	6.33	1.95–10.2	4.60
Eu/Eu*	1.0	0.8	0.6	0.6	0.52–0.70	0.66	0.61–0.87	0.73
Ba/Sr	1.0	3.6	3.8	4.7	0.7–13	2.2	0.4–4.0	1.5
Th/U	2.1	4.6	4.8	5.6	2.5–5.5	4.3	2.3–2.9	2.5
Zr/Hf	46	36	26	30	38–46	42	31–35	34
Zr/Th	48	22	10	19	16–70	21	20–77	36

Abbreviations: OIA, oceanic island arc; CIA, continental island arc; ACM, active continental margins; PM, passive margins. Eu/Eu* = $2 \times \text{Eu}_N / (\text{Sm}_N + \text{Gd}_N)$.

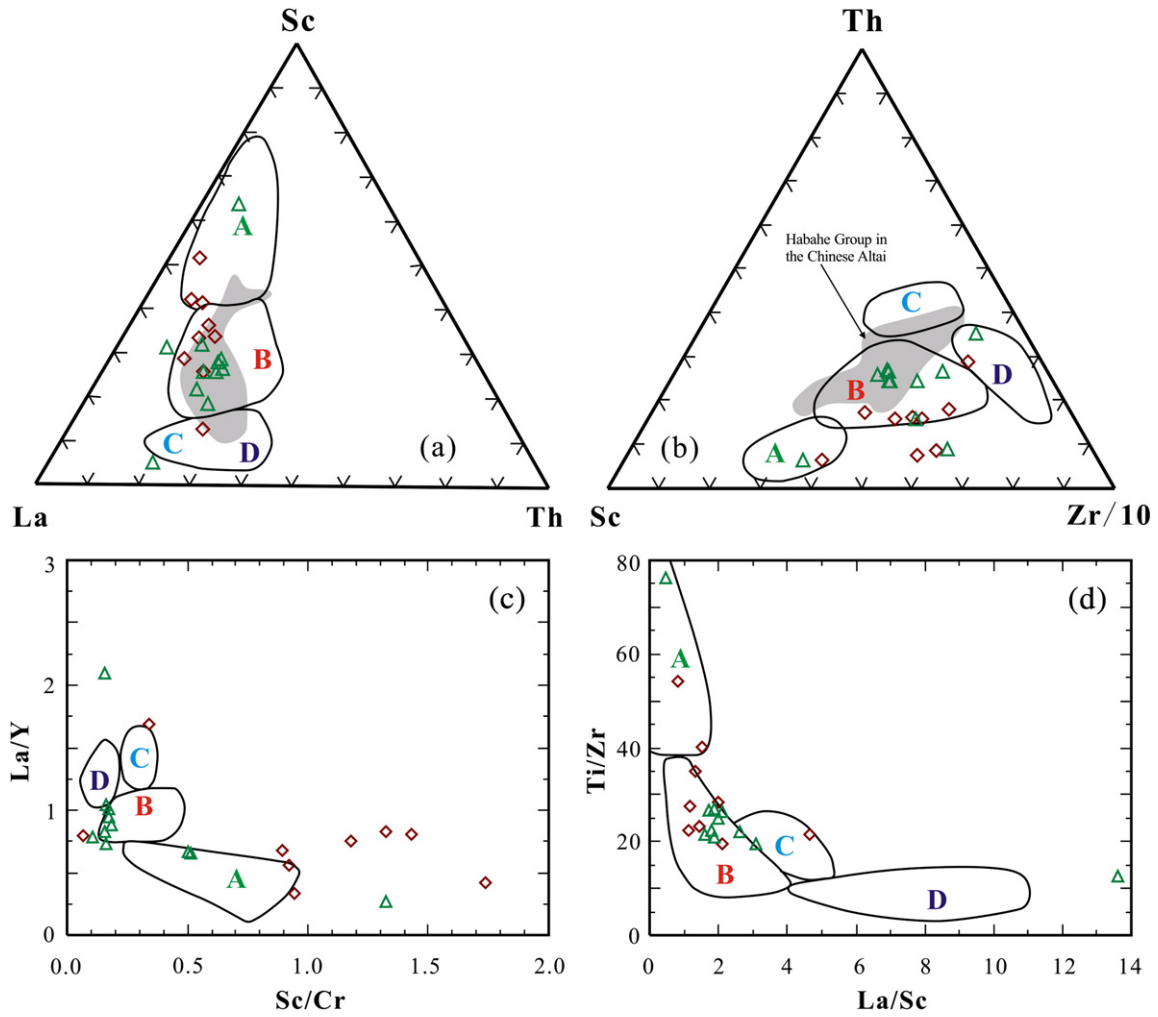


Fig. 10. Tectonic discriminating diagrams for the Paleozoic graywackes (after Roser and Korsch, 1986; Bhatia and Crook, 1986). Abbreviations for tectonic settings: A, oceanic island arc; B, continental arc; C, active continental margin; D, passive continental margin. Symbols are as in Fig. 3.

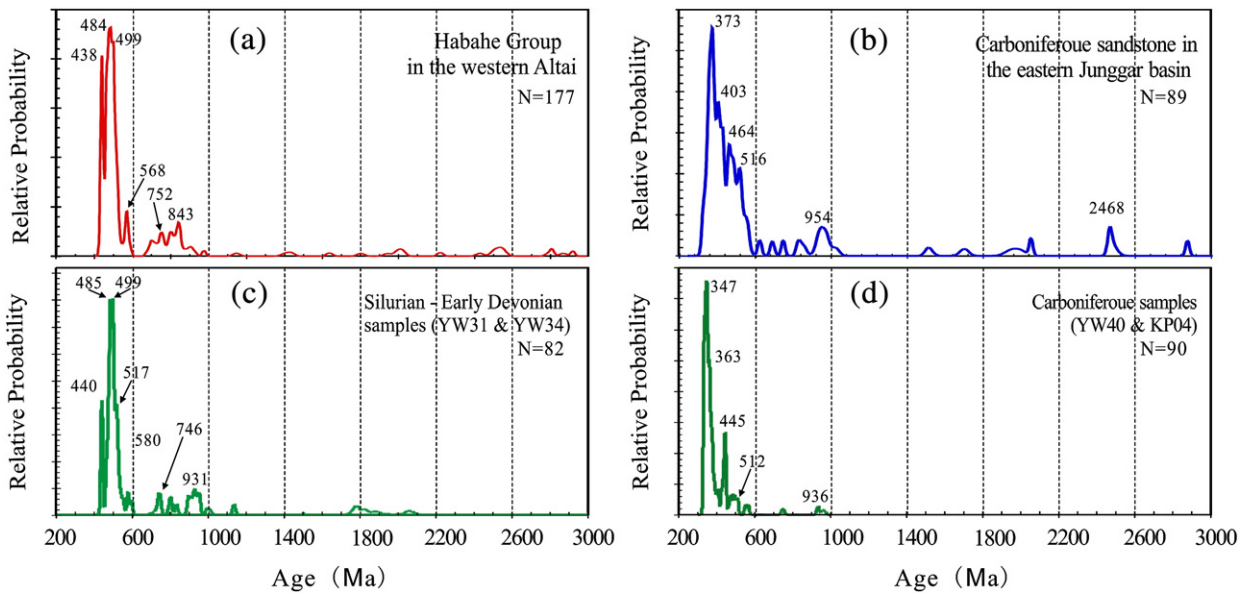


Fig. 11. Comparative relative probability plots for detrital zircons from the Paleozoic graywackes in the Chinese Altai and East Junggar. Original data: (a) from Long et al. (2010); (b) from Li et al. (2007); (c) and (d) from this study (data with disc.% >10 are excluded).

of Gondwana-derived terranes to form the Kazakhstan–Baikal composite continent which later collided with the Siberian continent (Dobretsov and Buslov, 2007; Buslov, 2011). In the southern CAOB, there are multiple linear accretionary orogenic collages consisting of terranes of different geodynamic origins, including Paleozoic arcs, ophiolites, accretionary wedges and microcontinents (Coleman, 1989; Xiao et al., 1992; Mossakovsky et al., 1993; Buchan et al., 2001; Yakubchuk et al., 2002; Buslov et al., 2004; Windley et al., 2007; Xiao et al., 2008, 2009). A branch of the PAO has been proposed to exist between East Junggar and the Chinese Altai, which is characterized by a Paleozoic ophiolite belt that includes the Kuerti and southern Qinghe ophiolites (Xu et al., 2003; Wu et al., 2006a, 2006b). SHRIMP U–Pb zircon dating of plagiogranite and basalt from these two ophiolites yielded $^{206}\text{Pb}/^{238}\text{U}$ ages of 372 ± 19 Ma and 352 ± 4 Ma, respectively (Zhang et al., 2003; Wu et al., 2006a, 2006b). These Paleozoic ages suggest that there was still a wide ocean between the two terranes in the Late Devonian to Early Carboniferous. However, the similar detrital zircon age spectra of Early Paleozoic sediments in East Junggar and the Chinese Altai imply that no ocean existed between them prior to their deposition (i.e., at 400–440 Ma). Given the similarity of the Early Paleozoic sediments in the two terranes and the absence of pre-Silurian basement rocks in the East Junggar terrane, we suggest that the pre-Silurian sedimentary rocks in East Junggar were part of the forearc accretionary complex of the Chinese Altai arc before the opening of the Kuerti and southern Qinghe oceans. In combination with the emplacement age of the Armantai and Kalamaili ophiolites, the age spectra of detrital zircons and the ages of igneous rocks in East Junggar, a three-phase tectonic model is proposed for the evolution of the southern CAOB involving a long-lasting northward subduction–accretion process accompanied by the opening of a back-arc basin. This model also provides insights into the history of the East Junggar and adjacent terranes (Fig. 12).

Phase (1) During Ordovician time (480–440 Ma), the Armantai Ocean, which was a branch of the southern PAO, subducted northward beneath the Chinese Altai arc (Fig. 12a). As parts

of the ocean floor, the present fragments of the Armantai ophiolite dominated by E-MORB and OIB-type basalts were not yet emplaced (Jin et al., 2001).

Phase (2) In the Silurian (440–400 Ma), a large sequence of accretionary complexes was formed along the southern margin of the Chinese Altai and the present fragments of the Armantai ophiolite were accreted into the previously formed accretionary complexes (Fig. 12b). The Yemaquan magmatic arc was built over the accretionary complexes by continuous subduction of the ocean floor. This interpretation is supported by the active continental margin tectonic setting and northward provenance of the pre-Early Paleozoic detrital zircons.

Phase (3) During a period from the Early Devonian to Early Carboniferous (400–330 Ma), the present fragments of the Kalamaili ophiolite were accreted onto the southern margin of the Yemaquan arc (Fig. 12c). Rollback of the subduction zone resulted in the formation of back-arc basins along the southern margin of the Chinese Altai, which are represented by the Kuerti and Qinghe ophiolites (Xu et al., 2003; Wu et al., 2006a, 2006b). Potential southward subduction of the oceanic floor of the back-arc basins is favored by the existence of coeval arc-related rocks in the Dulata magmatic arc (e.g., Mg-rich andesites, Nb-rich basalts, boninites, and adakites: Niu et al., 1999, 2006; Zhang et al., 2005), and in the formation of the Dulata magmatic arc to the north of the Yemaquan arc.

6. Conclusions

- (1) The Wuliegai Formation, the lowest subdivision of the HG, was deposited during a period from the Silurian to the Early Devonian (400–440 Ma). This suggests a younger depositional age for the HG than previously assumed. The KG and the uppermost subdivision of the HG were deposited after ~355 Ma

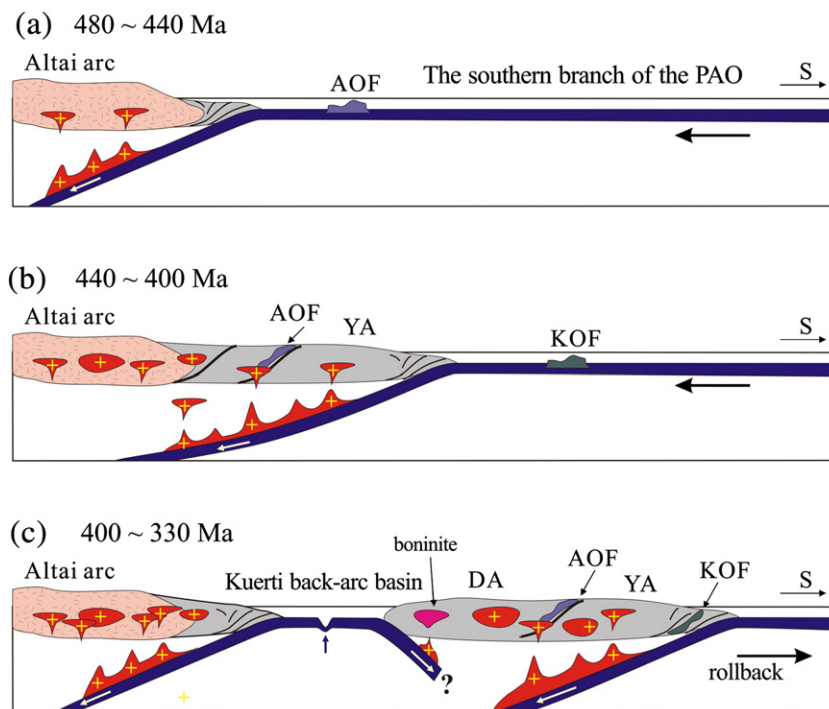


Fig. 12. Schematic diagrams illustrating the tectonic evolution of East Junggar and adjacent terranes. See text (Section 5, Discussion) for details. Abbreviations: AOF, Armantai ophiolite fragments; KOF, Kalamaili ophiolite fragments; YA, Yemaquan arc; DA, Dulata arc.

and can be incorporated into the Early Carboniferous Nanningshui Formation.

- (2) The Paleozoic graywackes in East Junggar were probably derived from an immature source dominated by felsic–andesitic igneous rocks and deposited at an active continental margin. Precambrian materials in the graywackes were derived from a source located to the north.
- (3) The Armantai ophiolite was probably emplaced prior to the Early Devonian, whereas the emplacement of the Kalamaili ophiolite postdates the Early Carboniferous.

Supplementary materials related to this article can be found online at [doi:10.1016/j.gr.2011.05.015](https://doi.org/10.1016/j.gr.2011.05.015).

Acknowledgments

We are very grateful to R.D. Nance and the three reviewers, whose polishing work and constructive comments have greatly improved the manuscript. This study was supported by the National Basic Research Program of China (2007CB411308), the National Natural Science Foundation of China (NSFC 40803009, 40725009 and 40721063) and the Hong Kong RGC (HKU704307P). We express our appreciation to K.J. Hou, Y. Liu and X.L. Tu for their laboratory assistance. This is contribution No. IS-1345 from GIGCAS.

Appendix A. Analytical methods

A.1. Geochemistry

Samples chosen for elemental and isotopic analysis were crushed into small pieces, ultrasonically cleaned in distilled water, then dried and powdered. Major element oxides (wt.%) were determined on fused disks with a 1:8 sample to $\text{Li}_2\text{B}_4\text{O}_7$ flux ratio, using a Rigaku ZSX100e X-ray fluorescence spectrometer at the Key Laboratory of Isotope Geochronology and Geochemistry, Guangzhou Institute of Geochemistry, Chinese Academy of Sciences. The accuracies of the XRF analyses are estimated to be ca. 1% for SiO_2 , ca. 5% for MnO and P_2O_5 and ca. 2% for other major oxides. The details of the analytical procedures were described by Li (1997). Trace elements, including the Rare Earth Element (REE), were analyzed using a Perkin-Elmer Sciex ELAN 6000 ICP-MS at the Guangzhou Institute of Geochemistry, Chinese Academy of Sciences following procedures described by Li et al. (2002) and Chen et al. (2010). The powdered samples (50 mg) were digested with mixed $\text{HNO}_3 + \text{HF}$ acid in steel-bomb coated Teflon beakers in order to assure complete dissolution of refractory minerals. An internal standard solution containing the single element Rh was used to monitor the signal drift. The USGS rock standards G-2, W-2, MRG-1 and AGV-1 and the Chinese national rock standards GSD-12, GSR-1, GSR-2 and GSR-3 were analyzed to calibrate the elemental concentrations of the measured samples. The analytical precision obtained was generally better than 5%. Table 1 shows major and trace element results of representative samples from the HG and KG.

A.2. Zircon separation and U–Pb dating

Detrital zircons were separated from the graywackes using conventional heavy liquid and magnetic techniques, and then selected by handpicking under a binocular microscope. Zircon grains were picked randomly and mounted on adhesive tape, then embedded in epoxy resin and polished to about half of their diameter. In order to observe the internal zonation pattern of the polished zircons, CL imaging was performed on a JXA-8100 Electron Probe Microanalyzer with a Mono CL3 Cathodoluminescence System for high resolution imaging and spectroscopy at the Guangzhou Institute of Geochemistry, Chinese Academy of Sciences. The zircon U–Pb dating was performed on a Thermo-Finnigan Neptune multi-collector ICP-MS

with a Newwave UP213 laser-ablation system at the Institute of Mineral Resources, Chinese Academy of Geological Sciences, Beijing. Pure helium was used as a carrier gas to enhance the transport efficiency of the ablated material. The analyses were performed with a beam diameter of 25 μm with a 10 Hz repetition rate and a laser power of $\sim 2.5 \text{ J/cm}^2$ (Hou et al., 2009). The masses of ^{206}Pb , ^{207}Pb , $^{204}(\text{Pb} + \text{Hg})$ and ^{202}Hg were measured in the ion-counting electron multiplier, while the masses of the more abundant isotopes of ^{208}Pb , ^{232}Th , ^{235}U and ^{238}U were collected by Faraday cup. The GJ1 zircon was used as a standard and the Plesovice zircon was used to optimize the machine. U, Th and Pb concentrations were calibrated using ^{29}Si as the internal standard and zircon M127 as the external standard (U: 923 ppm; Th: 439 ppm; Th/U: 0.475. Sláma et al., 2008). Subsequent data reduction was accomplished off-line ($^{207}\text{Pb}/^{206}\text{Pb}$ and $^{206}\text{Pb}/^{238}\text{U}$ ratios) using the ICPMS DataCal 4.3 program (Liu et al. 2008). Common-Pb can be considered negligible because of the low $^{206}\text{Pb}/^{204}\text{Pb}$ ratios (> 1000) for most of the analyzed spots (Wu et al., 2006a, 2006b). The Plesovice zircon was used as a secondary standard to check the accuracy of the analyses and yielded a $^{206}\text{Pb}/^{238}\text{U}$ age weighted mean of $337 \pm 2 \text{ Ma}$ (2SD, $n = 12$), which is in a good agreement with the ID-TIMS result ($^{206}\text{Pb}/^{238}\text{U}$ age = $337.13 \pm 0.37 \text{ Ma}$ (2SD), Sláma et al., 2008). Ages and concordia diagrams were calculated using Isoplot/Ex 3.0 (Ludwig, 2003). Since $^{206}\text{Pb}/^{238}\text{U}$ ratios generally provide more precise younger ages, whereas $^{207}\text{Pb}/^{206}\text{Pb}$ ratios provide more precise older ages, we used $^{206}\text{Pb}/^{238}\text{U}$ ages for zircons $< 1000 \text{ Ma}$ and $^{207}\text{Pb}/^{206}\text{Pb}$ ages for zircons $> 1000 \text{ Ma}$ (Gehrels et al., 2006; Supplementary Table A1).

References

- Badarch, G., Cunningham, W.D., Windley, B.F., 2002. A new terrane subdivision for Mongolia: implications for the Phanerozoic crustal growth of Central Asia. *Journal of Asian Earth Sciences* 21, 87–110.
- BGMRX (Bureau of Geology and Mineral Resources of Xinjiang Uygur Autonomous Region), 1993. Regional Geology of Xinjiang Uygur Autonomous Region. People's Republic of China, Ministry of Geology and Mineral Resources. Geological Memoirs, Series 1, No. 32. Geological Publishing House, Beijing, pp. 6–206. in Chinese.
- Bhat, M.L., Ghosh, S.K., 2001. Geochemistry of the 2.51 Ga old Rampur group pelites, western Himalayas: implications for their provenance and weathering. *Precambrian Research* 108, 1–16.
- Bhatia, M.R., Taylor, S.R., 1981. Trace-element geochemistry and sedimentary provinces: a study from the Tasman geosyncline, Australia. *Chemical Geology* 33, 115–125.
- Bhatia, M.R., 1983. Plate tectonics and geochemical composition of sandstones. *Journal of Geology* 91, 611–627.
- Bhatia, M.R., 1985. Rare earth element geochemistry of Australian Paleozoic graywackes and mudrocks: provenance and tectonic control. *Sedimentary Geology* 45, 97–113.
- Bhatia, M.R., Crook, K.A.W., 1986. Trace element characteristics of graywackes and tectonic setting discrimination of sedimentary basins. *Contributions to Mineralogy and Petrology* 92, 181–193.
- Bibikova, E.V., Kirnozova, T.I., Kozakov, I.K., et al., 1992. Polymetamorphic complexes of the southern slope of the Mongolia and Gobi Altai: results of U–Pb dating. *Geotektonika* 2, 104–112.
- Buchan, C., Cunningham, D., Windley, B.F., Tomurhuu, D., 2001. Structural and lithological characteristics of the Bayankhongor Ophiolite zone, central Mongolia. *Journal of the Geological Society London* 158, 445–460.
- Buslov, M.M., Saphonova, I.Yu., Watanabe, T., Obut, O.T., Fujiwara, Y., Iwata, K., Semakov, N.N., Sugai, Y., Smirnova, L.V., Kazansky, A.Yu., 2001. Evolution of the Paleo-Asian Ocean (Altai-Sayan Region, Central Asia) and collision of possible Gondwana-derived terranes with the southern marginal part of the Siberian continent. *Geoscience Journal* 5, 203–224.
- Buslov, M.M., Watanabe, T., Fujiwara, Y., Iwata, K., Smirnova, L.V., Safonova, I.Y., Semakov, N.N., Kiryanova, A.P., 2004. Late Paleozoic faults of the Altai region, Central Asia: tectonic pattern and model of formation. *Journal of Asian Earth Sciences* 23, 655–671.
- Buslov, M.M., 2011. Tectonics and geodynamics of the Central-Asian foldbelt: role of Late Paleozoic large-scale strike-slip faults. *Russian Geology and Geophysics* 52, 66–90.
- Cai, K.D., Sun, M., Yuan, C., Zhao, G.C., Xiao, W.J., Long, X.P., Wu, F.Y., 2010. Geochronological and geochemical study of mafic dykes from the northwest Chinese Altai: implications for petrogenesis and tectonic evolution. *Gondwana Research* 18, 638–665.
- Stratigraphy (Lithostratic) of Xinjiang Uygur autonomous region. In: Cai, T.X. (Ed.), Publishing house of college of geosciences, Wuhan, pp. 1–430 (in Chinese).
- Charvet, J., Shu, S.L., Laurent-Charvet, S., 2007. Paleozoic structural and geodynamic evolution of eastern Tianshan (NW China): welding of the Tarim and Junggar plates. *Episodes* 30, 162–186.

- Chen, B., Jahn, B.M., 2004. Genesis of post-collisional granitoids and basement nature of the Junggar Terrane, NW China: Nd–Sr isotope and trace element evidence. *Journal of Asian Earth Sciences* 23, 691–703.
- Chen, J.L., Xu, J.F., Wang, B.D., Kang, Z.Q., Li, J., 2010. Origin of Cenozoic alkaline potassic volcanic rocks at Konglongxiang, Lhasa terrane, Tibetan Plateau: products of partial melting of a mafic lower-crustal source? *Chemical Geology* 273, 286–299.
- Chen, S., Zhang, Y.Y., Guo, Z.J., 2009. Zircon SHRIMP U–Pb dating and its implications of post-collisional volcanic rocks in Santanghu Basin, Xinjiang. *Acta Petrologica Sinica* 25, 527–538 (in Chinese with English abstract).
- Coleman, R.G., 1989. Continental growth of northwest China. *Tectonics* 8, 621–635.
- Condie, K.C., 1993. Chemical composition and evolution of the upper continental crust: contrasting results from surface samples and shales. *Chemical Geology* 104, 1–37.
- Cox, R., Lowe, D.R., Cullers, R.L., 1995. The influence of sediment recycling and basement composition on evolution of mudrock chemistry in the southwestern United States. *Geochimica et Cosmochimica Acta* 59, 2919–2940.
- Cullers, R.L., 1994. The geochemical signatures of source rocks in size fractions of Holocene stream sediment derived from metamorphic rocks in the Wet Mountains region, USA. *Chemical Geology* 113, 327–343.
- Cullers, R.L., Podkovyrov, V.N., 2000. Geochemistry of the Mesoproterozoic Lakhanda shales in southeastern Yakutia, Russia: implications for mineralogical and provenance control, and recycling. *Precambrian Research* 104, 77–93.
- Cullers, R.L., Podkovyrov, V.N., 2002. The source and origin of terrigenous sedimentary rocks in the Mesoproterozoic Uj group, southeastern Russia. *Precambrian Research* 117, 157–1183.
- Darby, B.J., Gehrels, G.E., 2006. Detrital zircon reference for the North China block. *Journal of Asian Earth Sciences* 26, 637–648.
- Demoux, A., Kröner, A., Hegner, E., Badarch, G., 2009a. Devonian arc-related magmatism in the Tseel terrane of SW Mongolia: chronological and geochemical evidence. *Journal of the Geological Society, London* 166, 459–471.
- Demoux, A., Kröner, A., Liu, D.Y., Badarch, G., 2009b. Precambrian crystalline basement in southern Mongolia as revealed by SHRIMP zircon dating. *Int. J. Earth Sci.* 98, 1365–1380.
- Demoux, A., Kröner, A., Badarch, G., Jian, P., Tomurhuu, D., Wingate, M.T.D., 2009c. Zircon ages from the Baydrag Block and the Bayankhongor Ophiolite Zone: time constraints on Late Neoproterozoic to Cambrian subduction- and accretion-related magmatism in Central Mongolia. *The Journal of Geology* 117, 377–397.
- Dickinson, W.R., Gehrels, G.E., 2009. U–Pb ages of detrital zircons in Jurassic eolian and associated sandstones of the Colorado Plateau: evidence for transcontinental dispersal and intraregional recycling of sediment. *Geological Society of America Bulletin* 121, 408–433.
- Dobretsov, N.L., Buslov, M.M., Uchio, Y., 2004. Fragments of oceanic islands in accretion–collision areas of Gorny Altai and Salair, southern Siberia, Russia: early stages of continental crustal growth of the Siberian continent in Vendian–Early Cambrian time. *Journal of Asian Earth Sciences* 23, 673–690.
- Dobretsov, N.L., Buslov, M.M., 2007. Late Cambrian–Ordovician tectonics and geodynamics of Central Asia. *Russian Geology and Geophysics* 48, 1–12.
- Fedo, C.M., Nesbitt, H.W., Young, G.M., 1995. Unraveling the effects of potassium metasomatism in sedimentary rocks and paleosols, with implications for paleoweathering conditions and provenance. *Geology* 23, 921–924.
- Feng, R., Kerrich, R., 1990. Geochemistry of fine-grained clastic sedimentary rocks in the Archean Abitibi greenstone belt, Canada: implications for provenance and tectonic setting. *Geochim. Cosmochim. Acta* 54, 1061–1081.
- Feng, Y., Coleman, R.G., Tilton, G., Xiao, X., 1989. Tectonic evolution of the West Junggar region, Xinjiang, China. *Tectonics* 8, 729–752.
- Filippova, I.B., Bush, V.A., Didenko, A.N., 2001. Middle Paleozoic subduction belts: the leading factor in the formation of the Central Asian fold-and-thrust belt. *Russian Journal of Earth Sciences* 3, 405–426.
- Floyd, P.A., Leveridge, B.E., 1987. Tectonic environment of the Devonian Gramscatho basin, south Cornwall: framework mode and geochemical evidence from turbiditic sandstones. *Journal of the Geological Society of London* 144, 531–542.
- Gehrels, G.E., Yin, A., 2003. Detrital zircon geochronology of the northeastern Tibetan Plateau. *Geological Society of America Bulletin* 115, 881–896.
- Gehrels, G.E., Valencia, V., Pullen, A., 2006. Detrital zircon geochronology by laser-ablation multicollector ICPMS at the Arizona Laser-Chron Center. In: Olszewski, T., Huff, W. (Eds.), *Geochronology: Emerging Opportunities*. Philadelphia, Pennsylvania, Paleontological Society Short Course, pp. 1–10.
- Gerdes, A., Zeh, A., 2006. Combined U–Pb and Hf isotope LA–(MC–)ICP–MS analyses of detrital zircons: comparison with SHRIMP and new constraints for the provenance and age of an Armorican metasediment in Central Germany. *Earth and Planetary Science Letters* 249, 47–61.
- Griffin, W.L., Belousova, E.A., Shee, S.R., Pearson, N.J., O'Reilly, S.Y., 2004. Archean crustal evolution in the northern Yilgarn Craton: U–Pb and Hf isotope evidence from detrital zircons. *Precambrian Research* 131, 231–282.
- Han, C.M., Xiao, W.J., Zhao, G.C., Mao, J.W., Li, S.Z., Yan, Z., Mao, Q.G., 2006. Major types, characteristics and geodynamic mechanism of Upper Paleozoic copper deposits in northern Xinjiang, northwestern China. *Geology Reviews* 28, 308–328.
- He, G.Q., Li, J.Y., Hao, J., Li, J.L., Cheng, S.D., Xu, X., Xiao, X.C., Tian, P.R., Deng, Z.Q., Li, Y.A., Guo, F.X., 2001. Crustal Structure and Evolution of Xinjiang, China, Chinese National 305 Project 07-01. Urumqi, Xinjiang, China, pp. 1–227 (in Chinese).
- He, G.Q., 2004. *Tectonic Map of Xinjiang and Adjacent Areas, China (1:2500000)*. Geological Publishing House, Beijing.
- Helo, C., Hegner, E., Kröner, A., Badarch, G., Tomurtoogoo, O., Windley, B.F., Dulski, P., 2006. Geochemical signature of Paleozoic accretionary complexes of the Central Asian Orogenic Belt in South Mongolia: constraints on arc environments and crustal growth. *Chemical Geology* 227, 236–257.
- Hofmann, A., 2005. The geochemistry of sedimentary rocks from the Fig Tree Group, Barberton greenstone belt: implications for tectonic, hydrothermal and surface processes during mid-Archaean times. *Precambrian Research* 143, 23–49.
- Hou, K.J., Li, Y.H., Tian, Y.Y., 2009. In situ U–Pb zircon dating using laser ablation–multi ion counting–ICP–MS. *Mineral Deposits* 28, 481–492 (in Chinese with English abstract).
- Jahn, B.M., Wu, F., Chen, B., 2000. Granitoids of the Central Asian Orogenic Belt and continental growth in the Phanerozoic. *Transactions of the Royal Society of Edinburgh: Earth Science* 91, 181–193.
- Jahn, B.M., 2004. The Central Asian Orogenic Belt and growth of the continental crust in the Phanerozoic. In: Malpas, J., Fletcher, C.J.N., Ali, J.R., Aitchison, J.C. (Eds.), *Aspects of the Tectonic Evolution of China*, 226. Special Publications, London, pp. 73–100.
- Jian, P., Liu, D.Y., Zhang, Q., Zhang, F.Q., Shi, Y.R., Shi, G.H., Zhang, L.Q., Tao, H., 2003. SHRIMP dating of ophiolite and leucocratic rocks within ophiolites. *Earth Science Frontiers* 10, 439–456 (in Chinese with English abstract).
- Jin, C., Huang, X., Xu, Y., Li, Y., 2001. The Hongguleleng–Aermantai ophiolite and its relationship to mineralogy. In: Zhao, Z., Shen, Y., Tu, G. (Eds.), *Basic Research of the Metallogeny in Xinjiang*. Science in China, Beijing, pp. 27–51 (in Chinese).
- Kelty, T.K., Yin, A., Dash, B., Gehrels, G.E., Ribeiro, A.E., 2008. Detrital-zircon geochronology of Paleozoic sedimentary rocks in the Hangay–Hentey basin, north-central Mongolia: implications for the tectonic evolution of the Mongol–Okhotsk Ocean in central Asia. *Tectonophysics* 451, 290–311.
- Khain, E.V., Bibikova, E.V., Kröner, A., Zhuravlev, D.Z., Sklyarov, E.V., Fedotova, A.A., Kravchenko–Berezhnoy, I.R., 2002. The most ancient ophiolite of Central Asian fold belt: U–Pb and Pb–Pb zircon ages for the Dunzhungur Complex, Eastern Sayan, Siberia, and geodynamic implications. *Earth and Planetary Science Letters* 199, 311–325.
- Khain, E.V., Bibikova, E.V., Salnikova, E.B., Kröner, A., Gibsher, A.S., Didenko, A.N., Degtyarev, K.E., Fedotova, A.A., 2003. The Palaeo-Asian ocean in the Neoproterozoic and early Palaeozoic: new geochronologic data and palaeotectonic reconstructions. *Precambrian Research* 122, 329–358.
- Kozakov, I.K., Kotov, A.B., Salnikova, E.B., Bibikova, E.V., Kovach, V.P., Kirnozova, T.I., Berezhnaya, N.G., Lykhin, D.A., 1999. Metamorphic age of crystalline complexes of the Tuva–Mongolia Massif: the U–Pb geochronology of granitoids. *Petrology* 7, 177–191.
- Kozakov, I.K., Salnikova, E.B., Khain, E.V., Kovach, V.P., Berezhnaya, N.G., Yakovleva, N.G., Plotkina, Y.V., 2002. Early Caledonian crystalline rocks of the Lake zone, Mongolia: stages and tectonic environments as deduced from U–Pb and Sm–Nd isotopic data. *Geotectonics* 36, 156–166.
- Kozakov, I.K., Salnikova, E.B., Wang, T., Didenko, A.N., Plotkina, Y.V., Podkovyrov, V.N., 2007. Early Precambrian crystalline complexes of the Central Asian microcontinent: age, sources, tectonic position. *Strat. Geol. Corr.* 15, 121–140.
- Kuzmichev, A.B., Bibikova, E.V., Zhuravlev, D.Z., 2001. Neoproterozoic (800 Ma) orogeny in the Tuva–Mongolia Massif (Siberia): island arc–continent collision at the northeast Rodinia margin. *Precambrian Research* 110, 109–126.
- Kröner, A., Windley, B.F., Badarch, G., Tomurtoogoo, O., Hegner, E., Jahn, B.M., Gruschka, S., Khain, E.V., Demoux, A., Wingate, M.T.D., 2007. Accretionary growth and crust formation in the Central Asian Orogenic Belt and comparison with the Arabian–Nubian–Shield. *Geological Society America, Memoir* 200, 181–209.
- Kröner, A., Demoux, A., Zack, T., Rojas–Agramonte, Y., Jian, P., Tomurhuu, D., Barth, M., 2010. Zircon ages for a felsic volcanic rock and arc-related early Palaeozoic sediments on the margin of the Baydrag microcontinent, Central Asian Orogenic Belt, Mongolia. *Journal of Asian Earth Sciences*. doi:10.1016/j.jseas.2010.09.002.
- Li, J.Y., 1991. On evolution of Paleozoic plate tectonics of east Junggar, Xinjiang, China. In: Xiao, X.C., Tang, Y.Q. (Eds.), *On Tectonic Evolution of the Southern Margin of the Paleozoic Composite Megasuture Zone*. Beijing Technical Press, Beijing, pp. 92–108 (in Chinese).
- Li, J.Y., 1995. Main characteristics and emplacement processes of the East Junggar ophiolites, Xinjiang, China: *Acta Petrologica Sinica* 11 (Supplement), 73–84.
- Li, J.Y., Xiao, W.J., Wang, K.Z., 2003. Neoproterozoic–Paleozoic tectonostratigraphic framework of Eastern Xinjiang, NW China. In: Mao, J.W., Goldfarb, I.L., Seltmann, R., et al. (Eds.), *Tectonic Evolution and Metallogeny of the Chinese Altay and Tianshan*. IGCP 473 Workshop, Urumqi, International Association on the Genesis of Ore Deposits (IAGOD), CERAMS, Natural History Museum, London, pp. 31–74.
- Li, J.Y., 2004. Late Neoproterozoic and Paleozoic tectonic framework and evolution of eastern Xinjiang, NW China. *Geological Review* 50, 304–322 (in Chinese with English abstract).
- Li, J.Y., Yang, T.N., Li, Y.P., Zhu, Z.X., 2009. Geological features of the Karamaili faulting belt, eastern Junggar region, Xinjiang, China and its constraints on the reconstruction of Late Paleozoic ocean–continental framework of the Central Asian Region. *Geological Bulletin of China* 28, 1817–1826 (in Chinese with English abstract).
- Li, Y.P., Li, J.Y., Sun, G.H., Zhu, Z.X., Yang, Z.Q., 2007. Basement of Junggar basin: evidence from detrital zircons in sandstone of previous Devonian Kalamaili formation. *Acta Petrologica Sinica* 23, 1577–1590.
- Li, Z.H., Han, B.F., Song, B., 2004. SHRIMP zircon U–Pb dating of the Ertaipei granodiorite and its enclaves from eastern Junggar, Xinjiang, and geological implications. *Acta Petrologica Sinica* 20, 1263–1270.
- Li, X.H., 1997. Geochemistry of the Longsheng ophiolite from the southern margin of Yangtze Craton, SE China. *Geochemical Journal* 31, 323–337 (in Chinese with English abstract).
- Li, X.H., Liu, Y., Tu, X., Hu, G., Zeng, W., 2002. Precise determination of chemical compositions in silicate rocks using ICP–AES and ICP–MS: a comparative study of sample digestion techniques of alkali fusion and acid dissolution. *Geochimica* 31, 289–294 (in Chinese with English abstract).

- Liang, Y., Li, W., Li, W., Li, Y., 1999. Ophiolitic Emplacement Mechanism of Xinjiang: Xinjiang Geology 17, 344–349 (in Chinese with English abstract).
- Lin, J.F., Yu, H.X., Yu, X.Q., Di, Y.J., Tian, J.T., 2007. Zircon SHRIMP U–Pb dating and geological implication of the Sabei alkali-rich granite from Eastern Junggar of Xinjiang, NW China. *Acta Petrologica Sinica* 23, 1876–1884.
- Lin, J.F., Yu, H.X., Wu, C.Z., Su, W., Guo, J.F., 2008. Zircon SHRIMP U–Pb dating and geological implication of the Sabei Tin ore-deposit from Eastern Junggar of Xinjiang, China. *Geology in China* 35, 1197–1205 (in Chinese with English abstract).
- Liu, Y.S., Hu, Z.C., Gao, S., Günther, D., Xu, J., Gao, C., Chen, H., 2008. In situ analysis of major and trace elements of anhydrous minerals by LA-ICP-MS without applying an internal standard. *Chemical Geology* 257, 34–43.
- Long, X.P., Sun, M., Yuan, C., Xiao, W.J., Chen, H.L., Zhao, Y.J., Cai, K.D., Li, J.L., 2006. Genesis of carboniferous volcanic rocks in the Eastern Junggar: constraints on the closure of the Junggar Ocean. *Acta Petrologica Sinica* 22, 31–40.
- Long, X.P., Sun, M., Yuan, C., Xiao, W.J., Lin, S.F., Wu, F.Y., Xia, X.P., Cai, K.D., 2007. U–Pb and Hf isotopic study of zircons from metasedimentary rocks in the Chinese Altai: implications for Early Paleozoic tectonic evolution. *Tectonics* 26, TC5015, doi: 10.1029/2007TC002128.
- Long, X.P., Sun, M., Yuan, C., Xiao, W.J., Cai, K.D., 2008. Early Paleozoic sedimentary record of the Chinese Altai: implications for its tectonic evolution. *Sedimentary Geology* 208, 88–100.
- Long, X.P., Yuan, C., Sun, M., Xiao, W.J., Zhao, G.C., Wang, Y.J., Cai, K.D., Xia, X.P., Xie, L.W., 2010. Detrital zircon U–Pb ages and Hf isotopes of the early Paleozoic flysch sequence in the Chinese Altai, NW China: new constraints on depositional age, provenance and tectonic evolution. *Tectonophysics* 480, 213–231.
- Ludwig, K.R., 2003. User's Manual for Isoplot 3.00. A geochronological toolkit for Microsoft Excel, Berkeley Geochronology Center, Special Publication No. 4a, Berkeley, CA.
- Ma, R.S., Shu, L.S., Sun, J., 1997. Tectonic evolution and metallogeny of eastern Tianshan Mountains: Beijing, Geological Publishing House, pp. 1–202, in Chinese.
- Mao, Q.G., Xiao, W.J., Han, C.M., Yuan, C., Sun, M., 2008. Late Paleozoic south-ward accretionary polarity of the eastern Junggar orogenic belt: insight from the Dajiaoshan and other A-type granites. *Acta Petrologica Sinica* 24, 733–742.
- McLennan, S.M., Taylor, S.R., Kröner, A., 1983. Geochemical evolution of Archean shales from South Africa, I. the Swaziland and Pongola supergroups. *Precambrian Research* 22, 93–124.
- McLennan, S.M., Taylor, S.R., McCulloch, M.T., Maynard, J.B., 1990. Geochemical and Nd–Sr isotopic composition of deep-sea turbidites: crustal evolution and plate tectonic associations. *Geochimica et Cosmochimica Acta* 43, 375–388.
- McLennan, S.M., Taylor, S.R., 1991. Sedimentary rocks and crustal evolution: tectonic setting and secular trends. *Journal of Geology* 99, 1–21.
- McLennan, S.M., Hemming, S., McDaniel, D.K., Hanson, G.N., 1993. Geochemical approaches to sedimentation, provenance, and tectonics. *Geological Society of America Special Paper* 284, 21–40.
- Mossakovsky, A.A., Ruzhentsev, S.V., Samygin, S.G., Kheraskova, T.N., 1993. The Central Asian fold belt: geodynamic evolution and formation history. *Geotectonics* 26, 455–473.
- Nelson, D.R., 2001. An assessment of the determination of depositional ages for Precambrian clastic sedimentary rocks by U–Pb dating of detrital zircon. *Sedimentary Geology* 141–142, 37–60.
- Nesbitt, H.W., Young, G.M., 1982. Early Proterozoic climates and plate motions inferred from major element chemistry of lutites. *Nature* 199, 715–717.
- Niu, H., Xu, J., Yu, X., Chen, F., Zheng, Z., 1999. Discovery of the Mg-rich volcanics in Altay, Xinjiang, and its geological implications. *Chinese Science Bulletin* 44, 1685–1688 (in Chinese with English abstract).
- Niu, H.C., Sato, H., Zhang, H.X., Ito, J., Yu, X.Y., Nagao, T., Terada, K., Zhang, Q., 2006. Juxtaposition of adakite, boninite, high-TiO₂ and low-TiO₂ basalts in the Devonian southern Altay, Xinjiang, NW China. *Journal of Asian Earth Sciences* 28, 439–456.
- Ping, J., Dunyi, L., Yuruo, S., Fuqin, Z., 2005. SHRIMP dating of SSZ ophiolites from northern Xinjiang Province, China: implications for generation of oceanic crust in the Central Asian Orogenic Belt. In: Sklyarov, E.V. (Ed.), *Structural and Tectonic Correlation across the Central Asia Orogenic Collage: North-Eastern Segment*, Guidebook and Abstract Volume of the Siberian Workshop IGCP-480. IEC SB RAS, Irkutsk, p. 246.
- Ren, R., Han, B.F., Ji, J.Q., Zhang, L., Xu, Z., Su, L., 2011. U–Pb age of detrital zircons from the Tekes River, Xinjiang, China, and implications for tectonomagmatic evolution of the South Tian Shan Orogen. *Gondwana Research* 19, 460–470.
- Rojas-Agramonte, Y., Kröner, A., Demoux, A., Xia, X., Wang, W., Donskaya, T., Liu, D., Sun, M., 2011. Detrital and xenocryst zircon ages from Neoproterozoic to Palaeozoic arc terranes of Mongolia: significance for the origin of crustal fragments in the Central Asian Orogenic Belt. *Gondwana Research* 19, 751–763.
- Roser, B.P., Korsch, R.J., 1986. Determination of tectonic setting of sandstone-mudstone suites using SiO₂ content and K₂O/Na₂O ratio. *Journal of Geology* 94, 635–650.
- Safonova, I.Yu., Buslov, M.M., Iwata, K., Kokh, D.A., 2004. Fragments of Vendian–Early Carboniferous oceanic crust of the Paleo-Asian Ocean in foldbelts of the Altai–Sayan region of Central Asia: geochemistry, biostratigraphy and structural setting. *Gondwana Research* 7, 771–790.
- Safonova, I., Maruyama, S., Hirata, T., Kon, Y., Rino, S., 2010. LA ICP MS U–Pb ages of detrital zircons from Russia largest rivers: implications for major granitoid events in Eurasia and global episodes of supercontinent formation. *Journal of Geodynamics* 50, 134–153.
- Şengör, A.M.C., Natal'in, B.A., Burtman, V.S., 1993. Evolution of the Altai tectonic collage and Paleozoic crustal growth in Asia. *Nature* 364, 299–307.
- Şengör, A.M.C., Natal'in, B.A., 1996. Paleotectonics of Asia: fragments of a synthesis. In: Yin, A., Harrison, M. (Eds.), *The Tectonic Evolution of Asia*. Cambridge University Press, Cambridge, pp. 486–640.
- Shu, L.S., Lu, H.F., Charvet, J., Laurent, C.S., Yin, D.H., 2000. Paleozoic accretionary terranes in Northern Tianshan, NW China. *Chinese Geochemistry* 19, 193–202 (in Chinese with English abstract).
- Shu, L.S., Wang, Y.J., 2003. Late Devonian–Early Carboniferous radiolarian fossils from siliceous rocks of the Kelameili ophiolite, Xinjiang. *Geological Review* 49, 408–413.
- Sláma, J., Kosler, J., Condon, D.J., Crowley, J.L., Gerdes, A., Hancher, J.M., Horstwood, M.S.A., Morris, G.A., Nasdala, L., Norberg, N., Schaltegger, U., Schoene, B., Tubrett, M.N., Whitehouse, M.J., 2008. Plešovice zircon – a new natural reference material for U–Pb and Hf isotopic microanalysis. *Chemical Geology* 249, 1–35.
- Su, Y.P., Tang, H.F., Cong, F., 2008. Zircon U–Pb age and petrogenesis of the Huangyangshan alkaline granite body in East Junggar, Xinjiang. *Acta Mineralogica Sinica* 28, 117–126 (in Chinese with English abstract).
- Sun, G.H., Li, J.Y., Zhu, Z.X., Li, Y.P., Yang, Z.Q., 2007. Detrital zircon SHRIMP U–Pb dating of Carboniferous sandstone from the southern foot of the Harlik Mountains, eastern Xinjiang, and its geological implications. *Geology in China* 34, 778–789 (in Chinese with English abstract).
- Sun, S.-S., McDonough, W.F., 1989. Chemical and isotopic systematics of oceanic basalts: implications for mantle composition and processes. In: Saunders A. D. & Norry M. J. (eds), *Magmatism in the Ocean Basin*, Geological Society Special Publication. Blackwell Scientific Publications 42, 313–346.
- Sun, M., Yuan, C., Xiao, W., Long, X., Xia, X., Zhao, G., Lin, S., Wu, F., Kröner, A., 2008. Zircon U–Pb and Hf isotopic study of gneissic rocks from the Chinese Altai: progressive accretionary history in the early to middle Paleozoic. *Chemical Geology* 247, 352–383.
- Sun, M., Long, X.P., Cai, K.D., Jiang, Y.D., Wang, B.Y., Yuan, C., Zhao, G.C., Xiao, W.J., Wu, F.Y., 2009. Early Paleozoic ridge subduction in the Chinese Altai: insight from the marked change in Zircon Hf isotopic composition. *Science in China Series D: Earth Sciences* 52, 1345–1348.
- Tan, J.Y., Wu, R.J., Zhang, Y.Y., Wang, S.F., Guo, Z.J., 2009. Characteristics and geochronology of volcanic rocks of Batamayineishan Formation in Kalamaili, Eastern Junggar, Xinjiang. *Acta Petrologica Sinica* 25, 539–546.
- Tang, H.F., Su, Y.P., Liu, C.Q., Hou, G.S., Wang, Y.B., 2007. Zircon U–Pb age of the plagiogranite in Kalamaili belt, Northern Xinjiang and its tectonic implications. *Geotectonica et Metallogenia* 31, 110–117 (in Chinese with English abstract).
- Taylor, S.R., McLennan, S.M., 1985. *The Continental Crust: Its Composition and Evolution*. Blackwell Scientific Publications, Oxford, UK, pp. 312.
- Tong, Y., Wang, T., Hong, D.W., Dai, Y.J., Han, B.F., Liu, X.M., 2007. Ages and origin of the early Devonian granites from the north part of Chinese Altai Mountains and its tectonic implications. *Acta Petrologica Sinica* 23, 1933–1944.
- Wang, B.Y., Jiang, C.Y., Li, Y.J., Wu, H.E., Xia, Z.D., Lu, R.H., 2009. Geochemistry and tectonic implications of Karamaili ophiolite in East Junggar of Xinjiang. *Journal of Mineralogy and Petrology* 29 (3), 74–82 (in Chinese with English abstract).
- Wang, T., Hong, D.W., Jahn, B.M., Tong, Y., Wang, Y.B., Han, B.F., Wang, X.X., 2006. Timing, petrogenesis, and setting of Paleozoic synorogenic intrusions from the Altai Mountains, Northwest China: implications for the tectonic evolution of an accretionary orogen. *Journal of Geology* 114, 735–751.
- Wang, Y.J., Yuan, C., Long, X.P., Sun, M., Zhao, G.C., Xiao, W.J., Cai, K.D., Jiang, Y.D., 2010. Geochemistry, zircon U–Pb ages and Hf isotopes of the Paleozoic volcanic rocks in the northwestern Chinese Altai: petrogenesis and tectonic implications. *Journal of Asian Earth Sciences*. doi:10.1016/j.jseas.2010.11.005.
- Wang, Z.H., Sun, S., Li, J.L., Hou, Q.L., Qin, K.Z., Xiao, W.J., Hao, J., 2003. Paleozoic tectonic evolution of the northern Xinjiang, China: geochemical and geochronological constraints from the ophiolites. *Tectonics* 22, 1014. doi:10.1029/2002TC001396.
- Windley, B.F., Alexeiev, D., Xiao, W., Kröner, A., Badarch, G., 2007. Tectonic models for accretion of the Central Asian Orogenic Belt. *Journal of the Geological Society, London* 164, 31–47.
- Wu, B., He, G.Q., Wu, T.R., Li, H.J., Luo, H.L., 2006a. Discovery of the Buergen ophiolitic mélange belt in Xinjiang and its tectonic significance. *Geology in China* 33, 476–486 (in Chinese with English abstract).
- Wu, F.Y., Yang, Y.H., Xie, L.W., Yang, J.H., Xu, P., 2006b. Hf isotopic compositions of the standard zircons and baddeleyites used in U–Pb geochronology. *Chemical Geology* 234, 105–126.
- Xiao, W.J., Windley, B.F., Hao, J., Zhai, M.G., 2003. Accretion leading to collision and the Permian Solonker suture, Inner Mongolia, China: termination of the Central Asian Orogenic Belt. *Tectonics* 22, 1069. doi:10.1029/2002TC001484.
- Xiao, W.J., Windley, B.F., Badarch, G., Sun, S., Li, J., Qin, K., Wang, Z., 2004. Paleozoic accretionary and convergent tectonics of the southern Altaids: implications for the growth of central Asia. *Journal of the Geological Society of London* 161, 1–4.
- Xiao, W.J., Han, C.M., Yuan, C., Sun, M., Lin, S.F., Chen, H.L., Li, Z.L., Li, J.L., Sun, S., 2008. Middle Cambrian to Permian subduction-related accretionary orogenesis of North Xinjiang, NW China: implications for the tectonic evolution of Central Asia. *Journal of Asian Earth Sciences* 32, 102–117.
- Xiao, W.J., Windley, B.F., Yuan, C., Sun, M., Han, C.M., Lin, S.F., Chen, H.L., Yan, Q.R., Liu, D.Y., Qin, K.Z., Li, J.L., Sun, S., 2009. Paleozoic multiple subduction–accretion processes of the southern Altaids. *American Journal of Science* 309, 221–270.
- Xiao, W.J., Huang, B.C., Han, C.M., Sun, S., Li, J.L., 2010. A review of the western part of the Altaids: a key to understanding the architecture of accretionary orogens. *Gondwana Research* 18, 253–273.
- Xiao, X.C., Tang, Y.Q., Li, J.Y., Zhao, M., Feng, Y.M., Zhu, B.Q., 1990. On the tectonic evolution of the northern Xinjiang, Northwest China. *Geoscience of Xinjiang* 1, 47–68 (in Chinese with English abstract).
- Xiao, X., Tang, Y., 1991. Tectonic evolution of the southern margin of the Central Asian Complex megasuture belt: Beijing, Beijing Science and Technology Press, 6–25.

- Xiao, X., Tang, Y., Feng, Y., Zhu, B., Li, J., Zhao, M., 1992. Tectonic evolution of the Northern Xinjiang and its adjacent regions. Beijing, Geological Publishing House, 1–169 (in Chinese with English abstract).
- Xiao, Y., Zhang, H., Su, B., Sakyi, P.A., Lu, X., Yu, Y., Zhang, Z., 2011. Late Paleozoic Magmatic Record of East Junggar. Implication from zircon U–Pb dating and Hf isotope. *Gondwana Research*, NW China and its significance. doi:10.1016/j.gr.2010.12.008.
- Xu, J.F., Castillo, P.R., Chen, F.R., Niu, H.C., Yu, X.Y., Zhen, Z.P., 2003. Geochemistry of late Paleozoic mafic igneous rocks from the Kuerti area, Xinjiang, northwest China: implications for backarc mantle evolution. *Chemical Geology* 193, 137–154.
- Yakubchuk, A.S., Seltmann, R., Shatov, V., Cole, A., 2001. The Altaids: tectonic evolution and metallogeny. *Society of Economical Geologists Newsletters* 46, 7–14.
- Yakubchuk, A., Cole, A., Seltmann, R., Shatov, V., 2002. Tectonic setting, characteristics, and exploration criteria for gold mineralization in the Altaid orogenic collage: the Tien Shan province as a key example. *Society of Economical Geologists, Special Publication* 9, 177–201.
- Yakubchuk, A., 2004. Architecture and mineral deposit settings of the Altaid orogenic collage: a revised model. *Journal of Asian Earth Sciences* 23, 761–779.
- Yang, G.X., Li, Y.J., Si, G.H., Wu, H.E., Zhang, Y.Z., Jin, Z., 2008. LA-ICP-MS zircon U–Pb dating of the Kubusunan granodiorite in the Kalamaili area, eastern Junggar, Xinjiang. *Geology in China* 35, 849–858 (in Chinese with English abstract).
- Yang, G.X., Li, Y.J., Wu, H.E., Si, G.H., Jin, Z., 2009. LA-ICP-MS zircon U–Pb dating from granite-porphphy rocks in Xikuangbei, East Junggar, Xinjiang China. *Geological Bulletin of China* 28, 572–577 (in Chinese with English abstract).
- Yarmolyuk, V.V., Kovalenko, V.I., Salnikova, E.B., Kovach, V.P., Kozlovsky, A.M., Kotov, A.B., Lebedev, V.I., 2008. Geochronology of igneous rocks and formation of the late Paleozoic south Mongolian active margin of the Siberian continent. *Stratigraphy and Geological Correlation* 16, 162–181.
- Yuan, C., Xiao, W.J., Chen, H.L., Li, J.L., Sun, M., 2006. Zhaheba Potassic Basalt, Eastern Junggar (NW China): geochemical characteristics and tectonic implications. *Acta Geologica Sinica* 80 (2), 254–263 (in Chinese with English abstract).
- Yuan, C., Sun, M., Xiao, W.J., Li, X.H., Chen, H.L., Lin, S.F., Xia, X.P., Long, X.P., 2007. Accretionary orogenesis of the Chinese Altai: insights from Paleozoic granitoids. *Chemical Geology* 242, 22–39.
- Zhang, H.X., Niu, H.C., Terada, K., Yu, X.Y., Sato, H., Ito, J., 2003. Zircon SHRIMP U–Pb dating on plagiogranite from Kuerti ophiolite in Altay, North Xinjiang. *Chinese Science Bulletin* 48 (20), 2231–2235 (in Chinese with English abstract).
- Zhang, H.X., Niu, H., Sato, H., Yu, X.Y., Shan, Q., Zhang, B.Y., Ito, J., Nagao, T., 2005. Late Paleozoic adakites and Nb-enriched basalts from northern Xinjiang, northwestern China: evidence for the southward subduction of the Paleo-Asian Oceanic Plate. *Island Arc* 14, 55–68.
- Zhang, Z.C., Yan, S.H., Chen, B.L., Zhou, G., He, Y.K., Chai, F.M., He, L.X., Wan, Y.S., 2006. SHRIMP zircon U–Pb dating for subduction-related granitic rocks in the northern part of east Junggar, Xinjiang. *Chinese Science Bulletin* 51, 952–962.
- Zhang, Z.C., Mao, J.W., Cai, J.H., Zhou, G., Yan, S.H., Kusky, T.M., 2008. Geochemistry of picrites and associated lavas of a Devonian island arc in the Northern Junggar terrane, Xinjiang (NW China): implications for petrogenesis, arc mantle sources and tectonic setting. *Lithos* 105, 379–395.
- Zhang, Z.C., Zhou, G., Kusky, T.M., Yan, S.H., Chen, B.L., Zhao, L., 2009. Late Paleozoic volcanic record of the Eastern Junggar terrane, Xinjiang, Northwestern China: major and trace element characteristics, Sr–Nd isotopic systematics and implications for tectonic evolution. *Gondwana Research* 16, 201–215.
- Zheng, J.P., Sun, M., Zhao, G.C., Robinson, P.T., Wang, F.Z., 2007. Elemental and Sr–Nd–Pb isotopic geochemistry of Late Paleozoic volcanic rocks beneath the Junggar basin, NW China: implications for the formation and evolution of the basin basement. *Journal of Asian Earth Sciences* 29, 778–794.
- Zonenshain, L., Kuzmin, M.I., and Natapov, L.M., 1990. *Geology of the U.S.S.R.: a plate tectonic synthesis*. American Geophysical Union, *Geodynamics Series*, 21: 1–242.